Monthly Notices of the ROYAL ASTRONOMICAL SOCIETY

MNRAS **527,** 7263–7283 (2024) https://doi.org/10.1093/mnras/stad3515
Advance Access publication 2023 November 15

FASTCHEM COND: equilibrium chemistry with condensation and rainout for cool planetary and stellar environments

Daniel Kitzmann [1]★ Joachim W. Stock and A. Beate C. Patzer[2]

[1] *Center for Space and Habitability, University of Bern, Gesellschaftsstrasse 6, CH-3012 Bern, Switzerland*
[2] *Zentrum für Astronomie und Astrophysik (ZAA), Technische Universität Berlin (TUB), Hardenbergstraße 36, D-10623 Berlin, Germany*

Accepted 2023 November 12. Received 2023 November 9; in original form 2023 September 4

ABSTRACT

Cool astrophysical objects, such as (exo)planets, brown dwarfs, or asymptotic giant branch stars, can be strongly affected by condensation. Condensation not only directly affects the chemical composition of the gas phase by removing elements but the condensed material also influences other chemical and physical processes in these objects. This includes, for example, the formation of clouds in planetary atmospheres and brown dwarfs or the dust-driven winds of evolved stars. In this study, we introduce FASTCHEM COND, a new version of the FASTCHEM equilibrium chemistry code that adds a treatment of equilibrium condensation. Determining the equilibrium composition under the impact of condensation is complicated by the fact that the number of condensates that can exist in equilibrium with the gas phase is limited by a phase rule. However, this phase rule does not directly provide information as to which condensates are stable. A major advantage of FASTCHEM COND is its ability to automatically select the set stable condensates satisfying the phase rule. Besides the normal equilibrium condensation, FASTCHEM COND can also be used with the rainout approximation that is commonly employed in atmospheres of brown dwarfs or (exo)planets. FASTCHEM COND is available as open-source code, released under the GNU General Public Licence 3 (GPLv3). In addition to the C++ code, FASTCHEM COND also offers a PYTHON interface. Together with the code update, we also add about 290 liquid and solid condensate species to FASTCHEM.

Key words: astrochemistry – methods: numerical – planets and satellites: atmospheres – stars: atmospheres.

1 INTRODUCTION

Condensation is an important process in astrophysical objects that strongly affects the chemical composition of their gas phases. Typically, it can become very important at temperatures lower than roughly 2000 K, when the first, highly refractory species usually start to condensate out of the gas phase. Not only are the abundances of molecules directly affected by this process (e.g. Visscher & Fegley 2005), but the presence of condensing species also plays an important role in other physical and chemical processes in such objects.

For example, condensation in atmospheres of (exo)planets and brown dwarfs can lead to the formation of cloud particles that strongly impact the spectral appearance and temperature structures of these objects (e.g. Burrows & Sharp 1999; Ackerman & Marley 2001; Helling & Woitke 2006; Kitzmann et al. 2011; Morley et al. 2012; Lee et al. 2016; Gao et al. 2021). Moreover, the formation of dust grains in the atmospheres of asymptotic giant branch (AGB) stars, on the other hand, results in a massive stellar wind that finally leads to the loss of almost the entire stellar envelope to the interstellar medium over time (e.g. Hoefner et al. 1998; Winters et al. 2000; Gail & Sedlmayr 2013). Other environments where condensation is an important process are protostellar nebulae. For example, condensation sequences in the solar nebula are studied to determine the composition of planet-building blocks and meteorites (e.g. Fegley & Palme 1985; Palme & Fegley 1990; Lodders & Fegley 1993). Thus, the treatment of condensation and its impact on the gas phase composition in an equilibrium chemistry code is a fundamental necessity to achieve a deeper understanding of cooler astrophysical environments. An extensive overview of condensation in astrophysical environments and a summary of modelling efforts are discussed by, for example, Ebel (2006). More detailed discussion and a historical overview of the different approaches to the condensation problem and corresponding chemistry codes are provided by Lodders & Fegley (1997) or Ebel (2021).

The chemical equilibrium approximation simplifies the problem of describing condensate formation significantly, albeit at the expense of assuming local thermodynamic equilibrium. Although this assumption is not flawless, it remains reasonable for various scenarios. Nevertheless, this equilibrium is not attained in regions with very low pressures and temperatures, such as the outer circumstellar shells of AGB stars. In such an environment, for example, the time-scale of the hydrodynamic gas flow is much shorter than that of chemical reactions, resulting in a state where the chemical composition essentially becomes frozen (Gail & Sedlmayr 2013).

Yet, despite the inadequacy of chemical equilibrium condensation in certain environments, its computation remains a crucial necessity. Chemical equilibrium calculations establish a fundamental benchmark, serving as a foundation to extend computations to encompass kinetic effects on chemistry. Without knowledge of equilibrium

★ E-mail: daniel.kitzmann@unibe.ch

conditions for reference, it becomes unfeasible to ascertain whether a system is in or out of equilibrium, or to determine the degree of deviation from equilibrium (Ebel 2021).

Equilibrium chemistry calculations are typically done either via the law of mass action in combination with the element conservation equations (Brinkley 1946, 1947) or by using a Gibbs free energy minimization approach (White, Johnson & Dantzig 1957, 1958). Both formalisms yield the same solution but are numerically different (Zeleznik & Gordon 1960, 1968; van Zeggeren & Storey 1970; Smith & Missen 1982). The first forms a system of non-linear equations, while the latter is a global optimization problem. On the one hand, examples of computer codes that use the law-of-mass-action approach are CONDOR (Lodders & Fegley 1993), GGCHEM (Woitke et al. 2018), or FASTCHEM (Stock et al. 2018; Stock, Kitzmann & Patzer 2022). The Gibbs free energy minimization method, on the other hand, is implemented, for example, in the RAND method (White et al. 1958), the NASA-CEA code (Gordon & McBride 1994; McBride & Gordon 1996), SOLGAS and SOLGASMIX (Eriksson 1971, 1975), or STANJAN (Reynolds 1986). A more detailed overview and descriptions of the different numerical methods used to compute the chemical equilibrium composition can be found in, for example, Smith & Missen (1982) or van Zeggeren & Storey (1970).

Determining the equilibrium composition in a case where condensation occurs is quite more elaborate than a pure gas phase calculation since only a limited number of condensates can co-exist in equilibrium with the gas phase at the same time according to an extension of Gibbs' famous phase rule (Gibbs 1876; Denbigh 1955). In particular, it is in general not a priori obvious as to which species are stable. The phase rule only limits the number of stable condensates but does not restrict the potential combinations of condensates that can be present. This is especially problematic at low temperatures when many different species could in principle condense and, thus, the number of possible combinations could be very large.

Equilibrium condensation is therefore typically treated as a two-step process that includes solving for the combined gas–condensed phase chemical composition as well as finding the set of stable condensates. The latter step is often done in an iterative way by adding and/or removing potential condensates from a list of stable condensate candidates until the phase rule is satisfied and element conservation by the gas and condensed phase species is achieved (e.g. Gordon & McBride 1994; Woitke et al. 2018). Such iterative methods, however, become very challenging once the number of potential condensates is large. In such a case, additional a priori information on condensation sequences might be required to limit the number of combinations. While an iterative way is an established approach to solve this problem in astrophysical contexts, alternative methods do also exist (e.g. Leal et al. 2016).

The first two versions of our equilibrium chemistry code FASTCHEM focused solely on the gas phase chemistry. In the original publication (Stock et al. 2018), the basic semi-analytical approach that our chemistry code uses was introduced but was strictly limited to chemical systems including hydrogen. In FASTCHEM version 2 (Stock et al. 2022), we then, among other things, adapted the formalism to treat arbitrary element compositions.

In this study, we adapt FASTCHEM to include equilibrium condensation. With an internal version number of 3.0, we refer to this updated version as FASTCHEM COND. In addition to equilibrium condensation, FASTCHEM COND also employs the rainout approximation as an alternative condensation description that is commonly used in (exo)planetary science or for atmospheres of brown dwarfs (Marley et al. 2013). In Section 2, we first briefly summarize the theoretical concepts of equilibrium condensation and the related computational challenges. Section 3 describes the numerical framework implemented in FASTCHEM COND, while in Section 4 we test our new equilibrium chemistry code on a set of different scenarios from the literature that involve condensation.

2 THEORETICAL FRAMEWORK OF EQUILIBRIUM CONDENSATION

2.1 Gas phase treatment

Below, we very briefly summarize the equations describing chemical equilibrium in the gas phase using the law of mass action. For a more detailed description of the notation and formalisms used in the following, we refer to Stock et al. (2018, 2022).

The number density of gas phase species n_i is given by the law of mass action:

$$n_i = K_i(T) \prod_{j \in \mathcal{E}} {n_j}^{\nu_{ij}} , \qquad i \in \mathcal{S} \setminus \mathcal{E} , \tag{1}$$

where n_j is the number density of elements $j \in \mathcal{E}$ in their atomic form, K_i the temperature-dependent equilibrium constant of species i, and ν_{ij} their stoichiometric coefficients. The set $\mathcal{E}$ contains all elements, while the set $\mathcal{S}$ includes all gas phase species.

With the relative, normalized element abundances $\hat{\epsilon}_j$, the total number density of atomic nuclei of a given element $j \in \mathcal{E}$ is given by

$$N_j := \hat{\epsilon}_j n_{\langle \mathrm{g} \rangle} , \tag{2}$$

where the total number density of all atomic nuclei is defined by

$$n_{\langle \mathrm{g} \rangle} := \sum_{j \in \mathcal{E}} n_j + \sum_{j \in \mathcal{E}} \sum_{i \in \mathcal{S} \setminus \mathcal{E}} \nu_{ij} n_i . \tag{3}$$

We can then write the corresponding element conservation equation for element $j \in \mathcal{E}$:

$$N_j = n_j + \sum_{i \in \mathcal{S} \setminus \mathcal{E}} \nu_{ij} n_i . \tag{4}$$

Finally, assuming an ideal gas, the gas pressure p_g is given by

$$p_\mathrm{g} = k_\mathrm{B} T n_g = k_\mathrm{B} T \left(\sum_{j \in \mathcal{E}} n_j + \sum_{i \in \mathcal{S} \setminus \mathcal{E}} n_i \right) , \tag{5}$$

where k_B denotes Boltzmann's constant and T the gas temperature.

Equations (1), (4), and (5) form a system of linear and non-linear algebraic equations for the number densities of all gas phase species. The semi-analytical computational procedure used to solve this system is described in detail by Stock et al. (2022) (FASTCHEM 2).

2.2 Stoichiometric condensates

In the following, we only consider neutral, stoichiometric condensates.[1] Other cases, such as solid solutions, for example, are not considered here.

Let $\mathcal{C} = \{C_1, \ldots, C_{|\mathcal{C}|}\}$ be the set of all considered condensates in the chemistry model, where $|\mathcal{C}|$ denotes the total number of condensates.

[1]The term 'condensate' covers both solids and liquids throughout this work.

Unlike gas phase species described in the previous section, not all condensates can stably exist in equilibrium with the gas phase, but only a subset $\mathcal{C}_s \subset \mathcal{C}$. Depending on the chosen values for the temperature T, the gas pressure p_g, and the element abundances $\hat{\epsilon}_j$, $\mathcal{C}_s$ can also be an empty set, i.e. no condensate exists. This is the case for sufficiently high temperatures, for example. Furthermore, we introduce the subset of elements $\mathcal{E}_s \subset \mathcal{E}$ that are contained in the stable condensates $\mathcal{C}_s$.

The stability criterion of a condensate c can be expressed by using its activity a_c, given by the corresponding law of mass action (Gail & Sedlmayr 2013):

$$a_c = K_c(T) \prod_{j \in \mathcal{E}} n_j{}^{\nu_{cj}} , \qquad c \in \mathcal{C} , \tag{6}$$

where K_c is the equilibrium constant for the condensate.

For numerical computations, equation (6) can also be more conveniently expressed in its logarithmic form:

$$\ln a_c = \ln K_c(T) + \sum_{j \in \mathcal{E}} \nu_{cj} \ln n_j , \qquad c \in \mathcal{C} . \tag{7}$$

In the following, we will use this logarithmic form of the activity equation unless stated otherwise.

2.2.1 *Coupling of gas phase and condensates*

When condensates are taken into account, the element conservation equation is extended by a *fictitious* number density of condensed molecules n_c:

$$N_j = n_j + \sum_{i \in \mathcal{S} \setminus \mathcal{E}} \nu_{ij} n_i + \sum_{c \in \mathcal{C}_S} \nu_{cj} n_c , \qquad j \in \mathcal{E} , \tag{8}$$

where in analogy to equation (2), N_j is defined as

$$N_j := \hat{\epsilon}_j n_{\langle g \rangle} + \hat{\epsilon}_j n_{\langle c \rangle} , \tag{9}$$

with

$$n_{\langle c \rangle} := \sum_{j \in \mathcal{E}} \sum_{c \in \mathcal{C}_S} \nu_{cj} n_c . \tag{10}$$

This fictitious number density n_c should not be confused with an actual dust particle number density. On the contrary, the n_c is merely used in equation (8) to keep track of the elements bound in the condensed material. It is also important to note that the fictitious number densities of the condensates do not contribute to the pressure of the gas phase in equation (5).

An alternative way to describe the depletion of elements from the gas phase by condensates is the degree of condensation (see Gail & Sedlmayr 2013, for example), given by

$$f_j = \frac{1}{N_j} \sum_{c \in \mathcal{C}_S} \nu_{cj} n_c , \qquad j \in \mathcal{E} . \tag{11}$$

Using this degree of condensation, the effective element abundance ϕ_j in the gas phase can be expressed via

$$\phi_j = \left(1 - f_j\right) \epsilon_j , \qquad j \in \mathcal{E} , \tag{12}$$

where instead of ϵ_j, ϕ_j is then used to calculate the normalized element abundances $\hat{\epsilon}_j$.

With the element abundances without considering condensation, $\hat{\epsilon}_j(f_j = 0)$, and the total number density of atomic nuclei $n_{\langle g \rangle}$, we can also define the largest possible fictitious number density $n_{c,\max}$ of a condensate:

$$n_{c,\max} = \min_{\substack{j \in \mathcal{E} \\ \nu_{cj} > 0}} \left\{ \frac{n_{\langle g \rangle} \hat{\epsilon}_j(f_j = 0)}{\nu_{cj}} \right\} , \qquad c \in \mathcal{C} , \tag{13}$$

assuming that the least common element in a condensate is completely condensed.

2.2.2 *Stability criterion for condensates*

The activity equation (7) provides a stability criterion for condensates. For those that exist in equilibrium with the gas phase, the activity has to be $a_c = 1$ and, thus,

$$0 = \ln a_c = \ln K_c(T) + \sum_{j \in \mathcal{E}} \nu_{cj} \ln n_j , \qquad c \in \mathcal{C}_s . \tag{14}$$

All other (unstable) condensates have an activity of $a_c < 1$, yielding

$$0 > \ln a_c = \ln K_c(T) + \sum_{j \in \mathcal{E}} \nu_{cj} \ln n_j , \qquad c \in \mathcal{C} \setminus \mathcal{C}_s . \tag{15}$$

In chemical equilibrium therefore, only the following two different situations are permitted for all condensates:

(i) stable condensates, $c \in \mathcal{C}_s$: $\ln a_c = 0$, $n_c > 0$ and
(ii) unstable condensates, $c \in \mathcal{C} \setminus \mathcal{C}_s$: $\ln a_c < 0$, $n_c = 0$.

2.3 The phase rule

Equation (14) can be seen as constraints for the densities n_j of the elements $\mathcal{E}_s$ that are contained in stable condensates. Since the gas phase contains $|\mathcal{E}|$ unique elements, there is a maximum number of $|\mathcal{E}|$ in linearly independent equation (14). This a priori limits the number of stable condensates to $|\mathcal{C}_s| \leq |\mathcal{E}|$, which is usually a much smaller number than the total number of condensates $|\mathcal{C}|$ considered in a chemical system.

As described in Section 2.1, the n_j are the result of a system of non-linear equations involving the law of mass action for the gas phase species, the element conservation equations, and the ideal gas law. In a case that includes stable condensates, however, some n_j are also fixed by the solution of the equation (14). Consequently, they are therefore no longer free variables for the gas phase itself.

Thus, if all elements in the system are contained in stable condensates at the same time, their densities n_j in the gas phase are all determined by equation (14). The densities of all molecules are then directly given by their corresponding law of mass action with the fixed n_j following equation (1). This, however, creates the problem that the resulting n_i and n_j likely do not yield the correct pressure of the gas phase in equation (5) anymore.

Therefore, at least one incondensable element in the gas phase is needed, whose n_j is determined by the correct value of p_g. Consequently, the total number of stable condensates is effectively limited to $|\mathcal{C}_s| \leq |\mathcal{E}| - 1$.

This is an extension of the famous, so-called Gibbs' phase rule (Gibbs 1876, 1878; Denbigh 1955). While the phase rule limits the number of stable condensates, it unfortunately does not directly provide information on the condensates contained in the set $\mathcal{C}_s$, allowing for a potentially large number of possible combinations.

2.4 Solution strategies

One fundamental difference between the law of mass action for molecules (equation 1) in comparison to its formulation for condensates in equation (6) is that the former directly yields the number density of a molecule if the n_j are known, while the latter provides only a stability criterion. The number densities n_c appear only in the element conservation equation (equation 8) and the degree

of condensation (equation 11). Thus, there is no direct way of obtaining n_c.

This non-linear problem can be solved in a variety of different ways, two of which are briefly summarized in the following. For a broader overview of other methods, we refer the reader to van Zeggeren & Storey (1970). We note, however, that the two schemes discussed next both assume that the set of stable condensates $\mathcal{C}_s$ is already known when the non-linear system is solved.

2.4.1 *Iterative solution with Newton's method*

One possible solution for the coupled problem is to use an iteration based on Newton's method. This, for example, is done in the GGCHEM code by Woitke et al. (2018). Their model uses the effective element abundances $\hat{\epsilon}_j$ and the fictitious condensate number densities n_c as free variables.

Using equation (14) and the corresponding conservation equations for a considered set of stable condensates, GGCHEM assembles a linear system of equations to solve for the changes in the number densities n_c for given changes in the $\hat{\epsilon}_j$. This is coupled to the gas phase calculations with $\hat{\epsilon}_j$ in a Newton's method scheme until $a_c = 1$ is achieved for all considered condensates. In this case, the Jacobian matrix is not given analytically but is evaluated numerically by repeatedly calling the gas phase-only calculations.

A Newton's method is also used in the so-called NASA-method approach (Huff, Gordon & Morrell 1951).[2] In contrast to GGCHEM, however, the NASA method solves the gas and the condensed phase in a combined Newton's method rather than separating the computation into two distinct parts.

2.4.2 *Direct solution*

An alternative way is used in, for example, the CONDOR code by Lodders & Fegley (1993). Here, equation (14) for all considered, stable condensates is solved directly for the element densities n_j. Using these n_j in the gas phase calculations and comparing the results with those of the condensate-free case allows to obtain the degree of condensation f_j for all elements and, subsequently, the number densities n_c. No separate Newton's method is required here since the requirement of $a_c = 1$ is automatically satisfied by directly solving equation (14) and keeping the n_j fixed in the gas phase calculations.

2.4.3 *Deriving the set of stable condensates*

The two computational approaches discussed in the previous sections assume that the set of stable condensates is already known. Usually, however, this is rarely the case and the solution of this problem therefore has to be embedded in some form of iterative scheme.

A typical calculation would, thus, start with determining the gas phase composition in the absence of any condensates. This provides initial guesses for the n_j. Using these initial solutions, one can test for the potential presence of stable condensates by calculating their activities. If all a_c are smaller than unity, then no condensate can be present and the calculation is finished.

Else, if some condensates have activities larger than unity, one then has to find a solution in terms of the element number density n_j and the fictitious density n_c, such that the activities of all stable condensates are unity and the element conservation is fulfilled. The solution also has to agree with the phase rule and potentially stable condensates considered in the solution have to yield a linearly independent system of equations.

Especially at low temperatures, many different condensates can initially have activities $a_c > 1$ and, thus, are potential members of the set $\mathcal{C}_s$. This problem is commonly solved by constantly adding and removing condensates from $\mathcal{C}_s$, trying to solve the non-linear system with the methods described above (e.g. Gordon & McBride 1994; Woitke et al. 2018). This iteration has to continue until all condensates in $\mathcal{C}_s$ have an activity of $a_c = 1$, while all others have $a_c < 1$.

During the course of the iteration, it might become necessary to remove condensates again from the set $\mathcal{C}_s$, if, for example, they yield negative densities n_c. Considering, however, that many condensates compete for the same elements, it is not always immediately obvious as to which condensates need to be removed to stabilize the system.

Given the large number of possible combinations of stable condensates at low temperatures, finding the final set $\mathcal{C}_s$ is therefore extremely challenging without any prior knowledge. One possibility is to start at high temperatures and slowly cool down the system, using the results of the higher temperatures as initial guesses for the lower temperature calculations (e.g. Burrows & Sharp 1999). GGCHEM, for example, additionally creates a lookup table of the effective element abundances as a function of pressure and temperature that allows to obtain the results in later calculations more easily. This lookup table, however, obviously depends directly on the individual element abundances and needs to be created for every set of metallicity values.

3 CONDENSATE TREATMENT IN FASTCHEM

As illustrated in the previous section, solving the combined condensate–gas phase problem is challenging, especially under low-temperature conditions when many different condensates could potentially exist. The solution to this problem is made complicated by the fact that initially the final set of stable condensates $\mathcal{C}_s$ is not known. The phase rule and the requirement that the equation (14) for all considered condensates needs to be linearly independent offer some guidance. However, even with this supplementary information, an iterative approach of adding and removing condensates as described above does often not converge properly without further a priori information or good initial values for e.g. Newton's method (Burrows & Sharp 1999).

The necessity of selecting an initial set $\mathcal{C}_s$ is caused by the fact that equation (14) is only valid for stable condensates. Consequently, it is not possible to include all potential condensates at once in the system to derive the set $\mathcal{C}_s$ by solving the combined problem as evidently some of them might require a solution with $a_c < 1$ in case they are not stable.

In this new FASTCHEM version, we choose an alternative approach to this problem. This new approach is based on the basic ideas presented by Kulik et al. (2013) and Leal et al. (2016), the latter of which can be seen as a variant of the NASA method (Huff et al. 1951; van Zeggeren & Storey 1970). In the following, we adapt their equations and numerical methods to the general computational framework used in FASTCHEM.

3.1 Modified condensate equations

The most important modification of the standard approach is to adapt the activity equation in chemical equilibrium (equation 14), so that it is valid for *all* condensate species $\mathcal{C}$ instead of only for species

[2]The so-called NASA method by Huff et al. (1951) should not be confused with the NASA-CEA code (McBride & Gordon 1996). Both are based on very different computational methods: the former uses the law-of-mass-action approach, while the latter is based on the minimization of Gibbs free energy.

in the (initially unknown) set $\mathcal{C}_s$. This is achieved by introducing a correction factor $\lambda_c \geq 0$, such that

$$0 = \ln a_c + \lambda_c = \ln K_c(T) + \lambda_c + \sum_{j \in \mathcal{E}} \nu_{cj} \ln n_j \,, \qquad c \in \mathcal{C} \,. \quad (16)$$

Obviously, for stable condensates ($c \in \mathcal{C}_s$), the correction factor is $\lambda_c = 0$, while for the unstable ones ($c \in \mathcal{C} \setminus C_s$), we require $\lambda_c = -\ln a_c$ in equilibrium. As discussed by van Zeggeren & Storey (1970) and Leal et al. (2016), the new correction coefficients λ_c are directly connected to the Lagrange multipliers of the Gibbs free energy minimization approach (e.g. White et al. 1957, 1958).

Since a new variable λ_c is introduced, an additional equation is required to solve the combined system of equations. This auxiliary equation combines λ_c with the condensate number density n_c:

$$\lambda_c \, n_c = 0 \,. \quad (17)$$

This is supplemented by the element conservation equation, equation (8), involving all condensates.

The combined system ensures that the two possible states for equilibrium condensation are a natural outcome of the problem, i.e.

(i) $\lambda_c = 0 \Rightarrow \ln a_c = 0, n_c > 0 \,, \qquad c \in \mathcal{C}_s$ and
(ii) $\lambda_c > 0 \Rightarrow \ln a_c < 0, n_c = 0 \,, \qquad c \in \mathcal{C} \setminus \mathcal{C}_s.$

This approach, however, comes at the price of a larger system of equations, i.e. its dimension is in general $|\mathcal{E}| + 2\,|\mathcal{C}|$ instead of $|\mathcal{E}_s| + |\mathcal{C}_s|$.

For a numerical treatment, equation (17) needs to be adapted slightly. The constraint that either n_c or λ_c needs to be exactly equal to zero is numerically too strong. As suggested by Leal et al. (2016), the equation is therefore modified with a constant τ_c, such that

$$\lambda_c \, n_c = \tau_c \,, \qquad c \in \mathcal{C} \,. \quad (18)$$

The constant τ_c is a very small number, chosen such that it does not impact the outcome of calculation to a large degree. For τ_c, we use the expression

$$\tau_c = \tau \min_{\substack{j \in \mathcal{E} \\ \nu_{cj} > 0}} \left\{ N_j \right\} \,, \qquad c \in \mathcal{C} \,, \quad (19)$$

where τ is a small number with a default value of 10^{-15}. The quantity τ_c effectively controls the minimum non-zero number density of unstable condensates. The use of τ_c also implies that for stable condensates, $\ln a_c$ is not exactly zero but has a very small value of the order of τ.

Since both λ_c and n_c can become very small numbers, we use the logarithmic form of equation (18):

$$\ln \lambda_c + \ln n_c - \ln \tau_c = 0 \,, \qquad c \in \mathcal{C} \,. \quad (20)$$

In summary, we have to solve the following new, non-linear system of equations:

$$f_c^a := \ln K_c(T) + \lambda_c + \textstyle\sum_{j \in \mathcal{E}} \nu_{cj} \ln n_j = 0 \,, \qquad c \in \mathcal{C}, \quad (21)$$

$$f_c^\lambda := \ln \lambda_c + \ln n_c - \ln \tau_c = 0 \,, \; c \in \mathcal{C}, \quad (22)$$

$$f_j^e := N_j - n_j - \textstyle\sum_{i \in \mathcal{S} \setminus \mathcal{E}} \nu_{ij} n_i - \sum_{c \in \mathcal{C}} \nu_{cj} n_c = 0 \,, \; j \in \mathcal{E}, \quad (23)$$

for the unknown quantities n_j, n_c, and λ_c. Additionally, we require that all of these quantities have values larger than zero.

We note that the phase rule is never used explicitly in the construction of the system. Yet, the solution of the system of equations and, thus, the final set of stable condensates will automatically satisfy the phase rule. Furthermore, we also have not to pay any special attention to as to which condensates can be included to avoid linearly-dependent equations.

3.2 Newton's method

The combined system of equations (21), (22), and (23) introduced in the last section is solved by using Newton's method with an analytical Jacobian matrix. Instead of solving for the variables n_j, n_c, and λ_c, we replace them by their logarithmic counterparts $\ln n_j$, $\ln n_c$, and $\ln \lambda_c$. This provides a better numerical stability and also guarantees that these quantities cannot become negative.

For a Newton step k, we perform first-order Taylor series expansions of the functions f_c^λ, f_c^a, and f_j^e around the initial values $n_c^{(k)}$, $\lambda_c^{(k)}$, and $n_j^{(k)}$. For f_c^λ, this yields

$$\begin{aligned} 0 &= f_c^\lambda \left((n_c^{(k)}, \lambda_c^{(k)} \right) + \frac{\partial f_c^\lambda}{\partial \ln n_c} \Delta \ln n_c + \frac{\partial f_c^\lambda}{\partial \ln \lambda_c} \Delta \ln \lambda_c \\ &= \ln \lambda_c^{(k)} + \ln n_c^{(k)} - \ln \tau_c + \Delta \ln n_c + \Delta \ln \lambda_c \,, \end{aligned} \quad (24)$$

which can be rewritten as

$$b_c^\lambda = \Delta \ln n_c + \Delta \ln \lambda_c \,, \quad (25)$$

with

$$b_c^\lambda := \ln \tau_c - \ln \lambda_c^{(k)} - \ln n_c^{(k)} \,. \quad (26)$$

For the activity functions f_c^a, we perform the Taylor series expansion with respect to $\ln n_j$ and $\ln \lambda_c$:

$$\begin{aligned} 0 &= f_c^a \left(n_j^{(k)}, \lambda_c^{(k)} \right) + \sum_{j \in \mathcal{E}} \left(\frac{\partial f_c^a}{\partial \ln n_j} \Delta \ln n_j \right) + \frac{\partial f_c^a}{\partial \ln \lambda_c} \Delta \ln \lambda_c \\ &= \ln a_c^{(k)} + \lambda_c^{(k)} + \sum_{j \in \mathcal{E}} \nu_{cj} \Delta \ln n_j + \lambda_c^{(k)} \Delta \ln \lambda_c \,, \end{aligned} \quad (27)$$

where $\ln a_c^{(k)} = \ln a_c(\ln n_j^{(k)})$. This can also be written as

$$b_c^a = \sum_{j \in \mathcal{E}} \nu_{cj} \Delta \ln n_j + \lambda_c^{(k)} \Delta \ln \lambda_c \,, \quad (28)$$

with

$$b_c^a := -\ln a_c^{(k)} - \lambda_c^{(k)} \,. \quad (29)$$

A similar expansion for the element conservation equations f_j^e yields

$$\begin{aligned} 0 &= f_j^e \left(n_j^{(k)}, n_c^{(k)} \right) + \sum_{j' \in \mathcal{E}} \left(\frac{\partial f_j^e}{\partial \ln n_{j'}} \Delta \ln n_{j'} \right) + \sum_{c \in \mathcal{C}} \left(\frac{\partial f_j^e}{\partial \ln n_c} \Delta \ln n_c \right) \\ &= N_j - n_j^{(k)} - \sum_{i \in \mathcal{S} \setminus \mathcal{E}} \nu_{ij} n_i^{(k)} - \sum_{c \in \mathcal{C}} \nu_{cj} n_c^{(k)} \\ &\quad - \sum_{j' \in \mathcal{E}} \left(n_j^{(k)} \delta_{jj'} - \sum_{i \in \mathcal{S} \setminus \mathcal{E}} \nu_{ij} \nu_{ij'} n_i^{(k)} \right) \Delta \ln n_{j'} \\ &\quad - \sum_{c \in \mathcal{C}} \nu_{cj} n_c^{(k)} \Delta \ln n_c \,. \end{aligned} \quad (30)$$

Here, we have used the law of mass action (equation 1) to analytically calculate the derivatives of the species densities n_i with respect to those of the elements n_j and to express the number densities $n_i^{(k)}$ as a function of the initial element densities $n_j^{(k)}$. This can be rearranged

to

$$b_j^e = \sum_{j' \in \mathcal{E}} \left(n_j^{(k)} \delta_{jj'} + \sum_{i \in \mathcal{S} \setminus \mathcal{E}} \nu_{ij} \nu_{ij'} n_i^{(k)} \right) \Delta \ln n_{j'} + \sum_{c \in \mathcal{C}} \nu_{cj} n_c^{(k)} \Delta \ln n_c \,, \tag{31}$$

with

$$b_j^e := N_j - n_j^{(k)} - \sum_{i \in \mathcal{S} \setminus \mathcal{E}} \nu_{ij} n_i^{(k)} - \sum_{c \in \mathcal{C}} \nu_{cj} n_c^{(k)} \,. \tag{32}$$

The final system of equations then has the general form

$$\begin{pmatrix} \boldsymbol{I} & \boldsymbol{I} & \boldsymbol{0} \\ \boldsymbol{0} & \mathcal{J}_\lambda^a & \mathcal{J}_\mathcal{E}^a \\ \mathcal{J}_\mathcal{C}^e & \boldsymbol{0} & \mathcal{J}_\mathcal{E}^e \end{pmatrix} \cdot \begin{pmatrix} \Delta \ln n_\mathcal{C} \\ \Delta \ln \boldsymbol{\lambda}_\mathcal{C} \\ \Delta \ln n_\mathcal{E} \end{pmatrix} = \begin{pmatrix} b^\lambda \\ b^a \\ b^e \end{pmatrix} \,, \tag{33}$$

where $\boldsymbol{I}$ and $\boldsymbol{0}$ are the identity and zero matrix, respectively. The other components of the Jacobian matrix are given by the $|\mathcal{E}| \times |\mathcal{E}|$ matrix

$$\left(\mathcal{J}_\mathcal{E}^e\right)_{jj'} = n_j^{(k)} \delta_{jj'} + \sum_{i \in \mathcal{S} \setminus \mathcal{E}} \nu_{ij} \nu_{ij'} n_i^{(k)} \,, \tag{34}$$

the $|\mathcal{C}| \times |\mathcal{E}|$ matrix

$$\left(\mathcal{J}_\mathcal{E}^a\right)_{cj} = \nu_{cj} \,, \tag{35}$$

the $|\mathcal{E}| \times |\mathcal{C}|$ matrix

$$\left(\mathcal{J}_\mathcal{C}^e\right)_{jc} = \nu_{cj} n_c^{(k)} \,, \tag{36}$$

and the $|\mathcal{C}| \times |\mathcal{C}|$ diagonal matrix

$$\left(\mathcal{J}_\lambda^a\right)_{cc} = \lambda_c^{(k)} \,. \tag{37}$$

The components of the vector of unknowns are

$$\begin{aligned} (\Delta \ln n_\mathcal{C})_c &= \Delta \ln n_c, \\ (\Delta \ln \boldsymbol{\lambda}_\mathcal{C})_c &= \Delta \ln \lambda_c, \\ (\Delta \ln n_\mathcal{E})_j &= \Delta \ln n_j, \end{aligned} \tag{38}$$

while those of the right-hand-side vector are given by equations (26), (29), and (32). The total number of unknowns for this system is $2\,|\mathcal{C}| + |\mathcal{E}|$. Technically speaking, the system of equations is usually smaller than that because elements not forming any potentially stable condensate do not need to be included in the system.

With the computed solution for the quantities $\Delta \ln n_j$, $\Delta \ln n_c$, and $\Delta \ln \lambda_c$, the corresponding quantities are then corrected following

$$\ln x^{(k+1)} = \ln x^{(k)} + \Delta \ln x \,, \tag{39}$$

where x is either n_j, n_c, or λ_c. As mentioned earlier, the use of logarithmic quantities prevents these values from becoming negative or zero by construction.

3.3 Reduction of the system of equations

The system of equations (33) can become rather large if the number of potential condensates is very high, which typically happens at low temperatures. Its size, however, can be reduced significantly by removing both $\Delta \ln \lambda_c$ and $\Delta \ln n_c$ from the system of equations.

To remove $\Delta \ln \lambda_c$, we first solve equation (25) for $\Delta \ln \lambda_c$:

$$\Delta \ln \lambda_c = \ln \tau_c - \lambda_c^{(k)} - \ln n_c^{(k)} - \Delta \ln n_c \,. \tag{40}$$

In equation (28), we can now replace the quantity $\ln \Delta \lambda_c$, which yields

$$\hat{b}_c^a = \sum_{j \in \mathcal{E}} \nu_{cj} \Delta \ln n_j - \lambda_c^{(k)} \Delta \ln n_c \,, \tag{41}$$

with

$$\hat{b}_c^a := -\ln a_c^{(k)} - \lambda_c^{(k)} \left(1 + \ln \tau_c - \ln \lambda_c^{(k)} - \ln n_c^{(k)}\right) \,. \tag{42}$$

This reduces the linear system of equations to the form

$$\begin{pmatrix} -\mathcal{J}_\lambda^a & \mathcal{J}_\mathcal{E}^a \\ \mathcal{J}_\mathcal{C}^e & \mathcal{J}_\mathcal{E}^e \end{pmatrix} \cdot \begin{pmatrix} \Delta \ln n_\mathcal{C} \\ \Delta \ln n_\mathcal{E} \end{pmatrix} = \begin{pmatrix} \hat{b}^a \\ b^e \end{pmatrix} \tag{43}$$

for the $|\mathcal{C}| + |\mathcal{E}|$ unknowns $\Delta \ln n_c$ and $\Delta \ln n_j$. With the $\Delta \ln n_c$ from the solution of this system, we can then calculate the corresponding corrections $\Delta \ln \lambda_c$ from equation (40).

The same approach can be used for the unknowns $\Delta \ln n_c$ (Leal et al. 2016). Using equation (41), we can derive an equation for $\Delta \ln n_c$:

$$\begin{aligned} \Delta \ln n_c &= \frac{1}{\lambda_c^{(k)}} \sum_{j \in \mathcal{E}} \nu_{cj} \Delta \ln n_j - \frac{b_c^a}{\lambda_c^{(k)}} \\ &= \frac{1}{\lambda_c^{(k)}} \sum_{j \in \mathcal{E}} \nu_{cj} \Delta \ln n_j \\ &\quad + \frac{\ln a_c^{(k)}}{\lambda_c^{(k)}} + \ln \tau_c - \ln n_c^{(k)} - \ln \lambda_c^{(k)} + 1, \end{aligned} \tag{44}$$

and use it to eliminate $\Delta \ln n_c$ in equation (31). This yields a system of equations where the $\Delta \ln n_j$ are the only unknowns:

$$\hat{b}_j^e = \sum_{j' \in \mathcal{E}} \left(\left(\mathcal{J}_\mathcal{E}^e\right)_{jj'} + \sum_{c \in \mathcal{C}} \nu_{cj} \nu_{cj'} \frac{n_c^{(k)}}{\lambda_c^{(k)}} \right) \Delta \ln n_{j'} \,, \tag{45}$$

with the right-hand-side vector components

$$\hat{b}_j^e := b_j^e - \sum_{c \in \mathcal{C}} \nu_{cj} n_c^{(k)} \left(\frac{\ln a_c^{(k)}}{\lambda_c^{(k)}} + \ln \tau_c - \ln n_c^{(k)} - \ln \lambda_c^{(k)} + 1 \right) \,. \tag{46}$$

With the resulting $\Delta \ln n_j$, we can calculate the corrections $\Delta \ln n_c$ from equation (44) and subsequently again $\Delta \ln \lambda_c$ from equation (40).

Instead of the initial $|\mathcal{E}| + 2|\mathcal{C}|$ dimensions, the system of equations is now reduced to just $|\mathcal{E}|$ equations for the elements. Given that usually $|\mathcal{E}| \ll |\mathcal{C}|$, this provides a huge increase in computational performance.

Unfortunately, using this replacement for all condensates can yield a numerically unstable system. The reduced Jacobian matrix in equation (45) has terms of the form n_c/λ_c. For stable condensates, λ_c approaches values close to zero. In fact, with the original equation (17), we would effectively perform a division by zero here in case of stable condensates with $n_c \gg 1$. This generates very large, off-diagonal entries in the Jacobian, which can potentially make the matrix essentially numerically singular.

For unstable condensates, we have $n_c \approx 0$ and $\lambda_c \approx -\ln a_c$. In such a case, the problematic terms vanish from the Jacobian and the matrix remains well conditioned. Thus, while stable condensates have to be included in the Jacobian matrix for numerical stability, unstable ones can be safely removed. The system of equations would therefore have a dimension of $|\mathcal{C}_s| + |\mathcal{E}|$ once all unstable condensates have been identified and accordingly removed from the Jacobian matrix.

3.4 Numerical solution

To allow for more flexibility in the numerical calculations, FASTCHEM COND contains all three different systems of equations introduced so far. Before any of these systems of equations can be solved, the corresponding Jacobian matrix requires some rescaling to ensure

numerical stability. The different matrix components of the Jacobian imply that entries can potentially differ by many orders of magnitudes based on the current values of n_c, λ_c, or n_i. This can result in an unstable numerical behaviour. Before solving the system, each row of the matrix is therefore scaled by the inverse of its largest entry. Mathematically, this corresponds to the multiplication of the Jacobian with a non-singular, diagonal scaling matrix (cf. Deuflhard 2011) and usually leads to a well-conditioned Jacobian matrix.

We solve the system of equations directly by using an lower-upper (LU) decomposition with partial pivoting from the Eigen library.[3] This method provides a fast and stable way to obtain the solution. In principle, we could also exploit the fact that the Jacobian has a very sparse structure, since it contains more zero entries than non-zero ones. Thus, we could use iterative methods that have been especially designed for such systems with a sparse coefficient matrix. However, the overall dimension of our system is normally still quite small and these iterative methods therefore tend not to perform better than the direct solution via the LU decomposition.

In some cases, the system of equations can still become ill-conditioned, which makes a numerical solution challenging. Especially, the Jacobians for the reduced systems (33) and (45) are prone to become numerically singular. If, through the course of the Newton iterations, both n_c and λ_c for certain condensates become very small, the corresponding coupling terms in the submatrices $\mathcal{J}^e_{\mathcal{C}}$ and $\mathcal{J}^a_{\lambda}$ for these condensates are so small that they yield an almost singular matrix. This, of course, creates problems when using the LU decomposition with partial pivoting because this method a priori assumes that the matrix is invertible. Thus, the numerical solution for such an ill-conditioned system can in general not be trusted.

The full system (equation 33) is much less affected by these issues, since there are still coupling terms remaining in the Jacobian that stabilize the numerical solution. However, in rare cases, even the full Jacobian matrix can become ill-conditioned.

The Eigen library also offers, for example, an LU decomposition with full pivoting. While this method is slower than the version with partial pivoting, it can detect cases with singular matrices. FASTCHEM COND is able to use both solvers but by default employs the one with partial pivoting as it provides a much higher computational speed. The user can optionally choose the LU decomposition with full pivoting.

If FASTCHEM COND uses the method with full pivoting and detects a non-invertible matrix, it will either use a singular value decomposition to solve the system of equations or perturb the Jacobian to make it invertible (Dennis & Schnabel 1996). However, we note that both methods can lead to solutions that produce so minor corrections, such that the Jacobian matrix will remain non-invertible in the next iteration step. In that case, the iterative method in FASTCHEM COND will fail to converge. Consequently, in such a situation, it is usually advantageous to take a dampened Newton step into any random direction provided by the unstable LU decomposition. Most of the time this produces a well-conditioned matrix again in the next iteration step.

We also note that the full system of equations (33) is much less affected by a potentially singular Jacobian matrix. Even in the case of very small values for n_c and λ_c, there are still additional coupling terms left in the matrix to yield a stable matrix inversion. In fact, using the full system tends to require less iterations to converge than the reduced system of equations. However, the numerical cost per iteration step is much higher, which makes this approach overall often slower in terms of computational time. FASTCHEM COND will switch to this method if the iteration with the reduced system does not converge. The user can also optionally force FASTCHEM COND to always use the full Jacobian matrix in its calculations, which might help to overcome convergence issues.

[3] https://eigen.tuxfamily.org

3.5 Coupling with the gas phase chemistry

The condensation part of FASTCHEM COND, described above, needs to be iteratively coupled to the gas phase chemistry calculations. At the start of each coupled calculation, FASTCHEM will first determine the gas phase composition, neglecting any condensates. With that solution, the activities of all condensates are obtained. In case no activity is larger than unity, no stable condensates are possible and the calculation is finished.

If FASTCHEM finds some species, with initial a_c larger than one, it selects these condensates as potential candidates for the condensed phase and proceeds with the solution of the system described in the previous section. In principle, the mathematical description allows to include *all* condensates available in the chemical model, even those with activities smaller than unity. Since, however, those are not stable by definition, only condensates that can potentially be present are included in the calculation to limit the computational cost of solving the system of equations.

Having determined the set stable condensates and their corresponding densities n_c, the depletion of the elements from the gas phase is evaluated using the degree of condensation from equation (11) and the effective element abundances ϕ_j, $j \in \mathcal{E}_s$. In principle, one could now use these f_j and ϕ_j values to re-calculate the gas phase for all elements. However, at low temperatures, some of the f_j can become numerically exactly unity, which yields an effective element abundance of $\phi_j = 0$. Consequently, this can create numerical issues in the gas phase calculations for these elements.

Instead, we fix the number densities of the elements in their atomic form, n_j, in the gas phase calculations to the solution we obtain from the calculation of the condensed phase. As mentioned earlier, these n_j are essentially fixed by the solution of the activity equations and therefore should actually not be considered anymore as free variables in the gas phase.

An obvious advantage of using the second approach is that the calculation of the gas phase is simplified, since some elements do not need to be calculated at all as their n_j are already determined. This is especially helpful at lower temperatures when potentially many elements are taking part in condensation.

FASTCHEM COND will iteratively perform the calculations of the condensed and gas phase chemistry until the coupled system is converged. Normally, the first condensation iteration takes the longest time since this is the step where the selection of the stable and unstable condensates is made. Later calls of the condensation system typically need much fewer Newton steps because the sets of stable and unstable condensates usually do not change significantly. After each calculation of the gas phase, FASTCHEM COND checks for additional, potential condensates that need to be added to the system. The calculation proceeds until all condensates fulfil their stability criterion from Section 2.2.2 and all elements are conserved.

3.6 Rainout approximation

Besides the standard equilibrium condensation, FASTCHEM COND also supports calculations using the so-called rainout approximation. In the former case, each temperature and pressure point is treated individually. However, as pointed out by, for example, Lodders & Fegley

(2002) or Marley et al. (2013), this pure equilibrium condensation is not suitable for calculating the chemical composition of planetary atmospheres or brown dwarfs, because rainout affects the element distribution as function of altitude.

As discussed by Lodders & Fegley (2002), condensates in such high-gravity environments tend to form directly from the gas phase (*primary* condensates) that then settle into cloud layers. In a low-gravity case, such as a protoplanetary disc or a pre-stellar nebula, these primary condensates do not settle into distinct layers but remain dispersed in the gas phase. This allows for the formation of *secondary* condensates via chemical reactions between the gas phase and (primary) condensates when the temperature decreases further.

To simulate the rainout, FASTCHEM COND will first start the calculation at the lower boundary (highest pressure) for a given temperate–pressure profile $T(p)$ and work its way upwards towards lower pressures. If condensation is encountered at some pressure p, FASTCHEM COND will solve the coupled condensation and gas phase system as previously described. The converged system then yields the effective element abundances ϕ_j of the condensing elements left in the gas phase (see equation 12). Using these effective abundances, FASTCHEM will then change the actual element abundances ϵ_j to the computed ϕ_j at all pressures below the level where condensation occurred. This simulates the rainout of these elements into condensate layers and leads usually to a rapid decrease in the abundances of condensing elements in the upper parts of an atmosphere.

An example to illustrate the differences between equilibrium condensation and rainout is shown in Section 4.3 for an atmosphere of a brown dwarf.

3.7 Code update and availability

The numerical treatment for condensation and rainout described in the previous sections has been added to the FASTCHEM code. It is available as open source on GitHub (https://github.com/exoclime/FastChem). Like the previous versions of FASTCHEM, the code is released under the GNU General Public License version 3 (gnu.org 2007). This new FASTCHEM release has a version number of 3.0 and is referred to as FASTCHEM COND. We note that for calculations not involving condensation, the results of FASTCHEM COND are identical to those calculated with the previous version FASTCHEM 2.

As described by Stock et al. (2022), FASTCHEM is written mainly in object-oriented C++ but additionally offers a PYTHON interface (PYFASTCHEM) that allows it to be imported as a normal PYTHON module. Some example PYTHON scripts are included in the repository that showcase the use of FASTCHEM COND for several different scenarios. In addition to the GitHub repository, PYFASTCHEM is also available as a PYPI package that can easily be installed via `pip`.

The PYTHON interface of FASTCHEM COND has been adapted to account for calculations involving condensates. New parameter options have also been included in the interface that allow the user to access special internal parameters. A detailed description of the C++ code and the PYTHON interface is available in the manual, located in the GitHub repository.

Thermochemical data for condensates mostly based on the Joint Army-Navy-Air Force (JANAF) Thermochemical Tables (Chase 1998) have been added to FASTCHEM COND. In particular, the current version of FASTCHEM COND includes about 290 solids and liquids for 27 elements more abundant than germanium for the solar element abundances by Asplund et al. (2009). Details on the condensate data can be found in Appendix A. We aim to add more elements, gas phase species, and condensates in future releases of FASTCHEM.

4 TEST CALCULATIONS

In this section, we test the new condensation approach in FASTCHEM COND for three different scenarios of astrophysical interest. In the first case, we replicate the equilibrium condensation calculations from Sharp & Huebner (1990). In the second scenario, we evaluate the numerical stability of our new code by calculating the equilibrium condensation in a protoplanetary disc. Since the temperatures within the disc drop to values of roughly 10 K, this scenario presents a numerically very challenging case. In the last scenario, we show the differences in the chemical composition between a standard equilibrium condensation calculation and the rainout approximation for the atmosphere of a brown dwarf. All results shown in the following can be easily reproduced by the PYTHON scripts contained in the FASTCHEM repository.

4.1 Comparison with Sharp & Huebner (1990)

The study by Sharp & Huebner (1990) focuses on the chemical composition of the gas phase under the influence of condensation in a general astrophysical context. They adapted the SOLGASMIX code (Eriksson 1971; Besmann 1977) to include the condensation of species for solar element abundances. In contrast to FASTCHEM COND, SOLGASMIX used a Gibbs free energy minimization approach to solve the equilibrium condensation problem. The study presents the resulting gas phase composition as a function of temperature for a fixed pressure of 0.5 bar.

For this test calculation, we replicate the temperature and pressure conditions used by Sharp & Huebner (1990). The resulting abundances of selected gas phase species are shown in the plots of Fig. 1, which roughly mirror those presented by Sharp & Huebner (1990). We note, however, that we extended the temperature range of the chemistry calculations to even lower temperatures than those used by Sharp & Huebner (1990) to illustrate the numerical capabilities of our new code.

Comparing our results with those of Sharp & Huebner (1990) suggests a very good agreement in terms of the resulting molecular abundances. Minor changes can be explained by the different element abundances. Sharp & Huebner (1990) employed element abundances based on Cameron (1973), wheres FASTCHEM COND uses the ones from Asplund et al. (2009). Other notable differences are the different sets of gas phase species and condensates as well as the underlying thermochemical data the fitted equilibrium constants are based on.

In addition to the gas phase, we also show the degree of condensation for several elements in Fig. 2. The results indicate that most species condense out completely below a certain temperature. Because oxygen is much more abundant than the other more refractory elements, only about 20 per cent of O is condensed out until the lowest considered temperature of 500 K. For a solar element abundance mixture, oxygen would condense out almost completely at even lower temperatures in the form of water ice.

Examples for the condensation sequences of titanium- and magnesium-bearing condensates are shown in Fig. 3. Titanium first condenses into the high-temperature condensate perovskite [$CaTiO_3$(s)]. At lower temperatures, Ti then switches to titanium oxide condensates, namely Ti_3O_5, Ti_4O_7, and TiO_2. The transitions between the different Ti condensates are very sharp, suggesting that titanium is only present in a single condensate at a time.

In contrast, magnesium can be found in several stable condensates simultaneously as suggested by the lower panel of Fig. 3. It first condenses into spinel ($MgAl_2O_4$), followed shortly afterwards by diopside ($CaMgSi_2O_6$) and forsterite (Mg_2SiO_4). Lastly, magne-

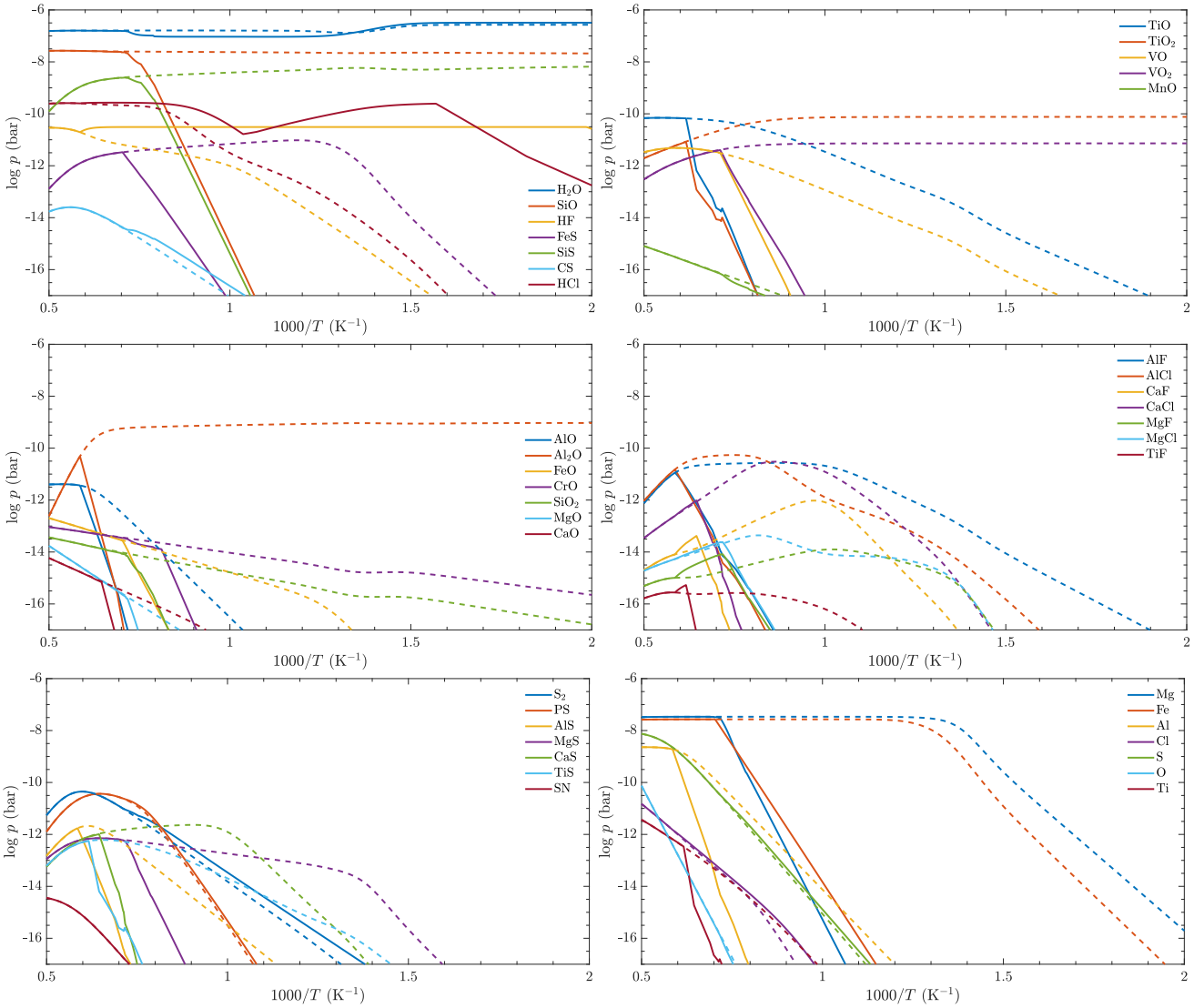

Figure 1. Comparison with equilibrium condensation calculations of Sharp & Huebner (1990). The plots show the partial pressures of gas phase species as a function of temperature and roughly mirror the results shown by Sharp & Huebner (1990) with some species moved to other panels for better visualization. We note that our calculations extend to lower temperatures than those presented by Sharp & Huebner (1990). Following the corresponding figures by Sharp & Huebner (1990), solid lines refer to the chemistry calculations with equilibrium condensation while dashed lines refer to those without.

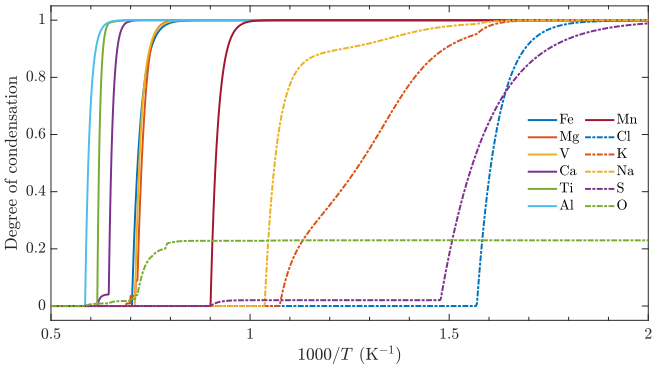

Figure 2. Degree of condensation for selected elements for the Sharp & Huebner (1990) scenario as a function of temperature and a gas pressure of $p_g = 0.5$ bar.

sium also condenses into enstatite ($MgSiO_3$), which competes with forsterite for the most abundant magnesium-bearing condensate. In contrast to the titanium condensation sequence, none of the magnesium condensates actually disappear after they have formed, though their abundances can change as a function of temperature.

4.2 Protoplanetary disc

In this section, we test our updated FASTCHEM code on a temperature–pressure structure of the mid-plane of a protoplanetary disc. The temperature and pressure profile is based on the disc model described in Emsenhuber et al. (2021) and Weder, Mordasini & Emsenhuber (2023) and shown in Fig. 4. Throughout the disc, the pressure varies by more than 14 orders of magnitude, from about 10^{-3} to 10^{-17} bar. The temperature starts at roughly 1700 K near the central star and drops to values of almost 10 K in the outermost part of the disc. The low temperatures and densities, especially at larger distances, make this scenario numerically very challenging. In the outer parts of the

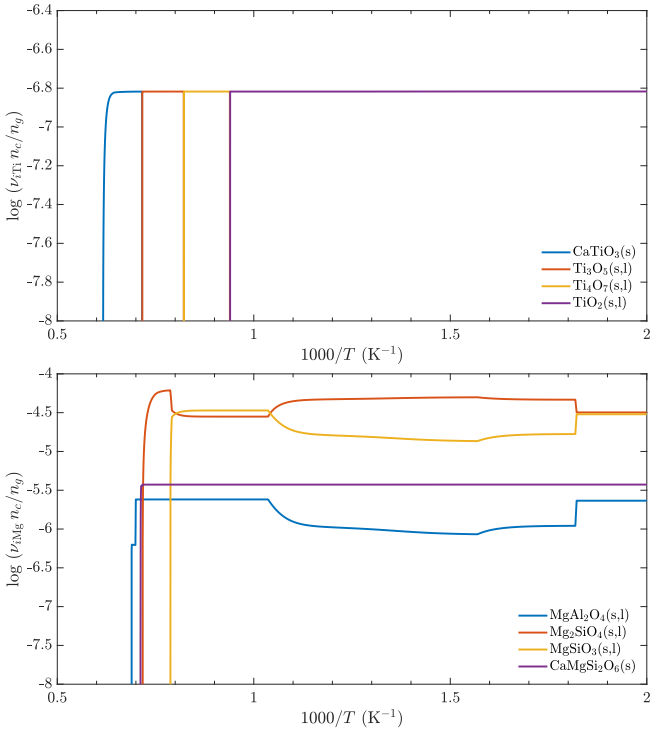

Figure 3. Examples for condensation sequences of selected elements for the Sharp & Huebner (1990) scenario. The upper panel shows titanium-bearing condensates, while the lower panel depicts the condensation sequence for magnesium.

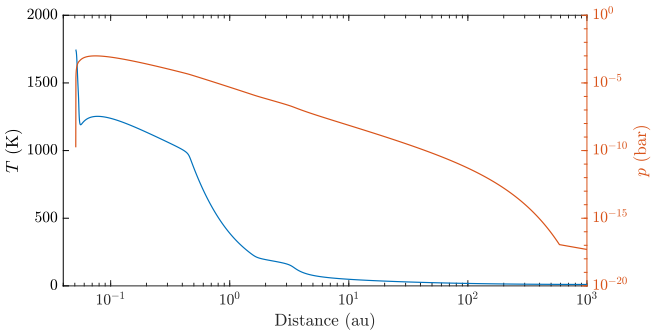

Figure 4. Temperature (left) and pressure (right) profiles of the mid-plane of a protoplanetary disc as a function of distance from the central star. The profiles are based on calculations with the disc model described in Emsenhuber et al. (2021) and Weder et al. (2023).

disc, essentially all condensates considered in FASTCHEM COND have initially activities larger than unity, which makes it obviously quite difficult to obtain the final set of stable condensates according to the phase rule.

We note that this calculation is only done to test the numerical stability of the chemistry and condensation scheme and not to properly model the chemical composition of a protoplanetary disc. In reality, the disc chemistry is rather complex, involving various additional chemical and physical processes, such as photoevaporation, for example (see e.g. Henning & Semenov 2013). For the calculations here, we also removed germanium from the list of considered elements, because currently Ge has no associated gas phase molecules or condensates due to the lack of corresponding data in the JANAF tables (Chase 1998).

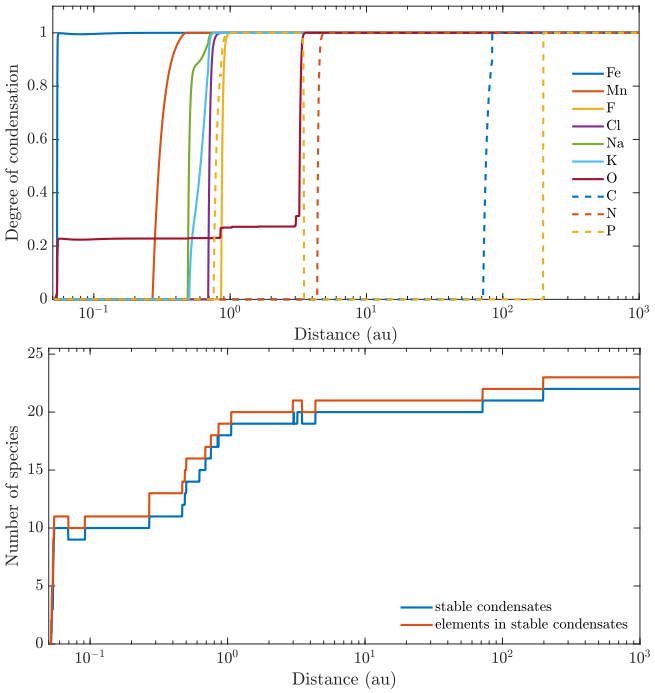

Figure 5. Degree of condensation of selected elements (upper panel) and the number of stable condensates (lower panel) as a function of the distance from the central star for the protoplanetary disc. The lower panel also additionally shows the total number of elements contained in stable condensates to verify that the results satisfy the phase rule.

Table 1. List of stable condensates in the outer parts of the protoplanetary disc with the associated elements according to the phase rule.

Stable condensate	Associated element	$n_c/n_{c,\max}$
Al_2SiO_5(s)	Al	0.35
NH_4Cl(s)	Cl	1.0
Co(s)	Co	1.0
Cr_2O_3(s, l)	Cr	1.0
Cu(s, l)	Cu	1.0
MgF_2(s, l)	F	1.0
FeS(s, l)	S	0.9
$Mg(OH)_2$(s)	Mg	0.63
$MgSiO_3$(s, l)	Si	0.37
$Mg_3P_2O_8$(s, l)	P	1.0
Ni_3S_2(s, l)	Ni	1.0
TiO_2(s, l)	Ti	1.0
V_2O_3(s, l)	V	1.0
Zn(s, l)	Zn	1.0
MnS(s)	Mn	1.0
Fe_2SiO_4(s)	Fe	0.63
$CaMgSi_2O_6$(s)	Ca	1.0
$KAlSi_3O_8$(s)	K	1.0
$NaAlSi_3O_8$(s)	Na	1.0
H_2O(s, l)	O	0.68
CH_4(s, l)	C	1.0
NH_3(s, l)	N	0.99

In total, this calculation included 26 elements. Thus, following the phase rule, a maximum of 25 different condensates should be able to co-exist at most. As the lower panel of Fig. 5 shows, the highest number of stable condensates in our calculation reaches a value of 22 in the outer disc (see Table 1), clearly satisfying the phase rule. The number of stable condensates should also not be higher than the

number of elements contained in them. In our case, the converged system also satisfies this requirement.

The upper panel of Fig. 5 shows the degree of condensation of selected elements as a function of distance (upper panel). Just like in the previous case of Sharp & Huebner (1990), elements tend to completely condense out below a certain temperature. Iron is lost from the gas phase very close to the inner disc boundary. The same also applies to other elements contained in high-temperature condensates, such as Ca or Al (not shown). More volatile elements, such as Mn, Na, K, or Cl, start to condense at distances between 0.3 and 1 au. Oxygen is also contained in many of the high-temperature condensates. Due to the high element abundance of O compared to the other elements, only about 20 per cent of the element is lost from the gas phase at small distances, though. However, once the temperature–pressure profile crosses the water ice line of the protoplanetary disc, oxygen condenses out completely into H_2O(s) at distances larger than roughly 3.5 au.

In the outer part of the disc, only hydrogen and the noble gases argon, neon, and helium remain in the gas phase. Hydrogen is also contained in some condensates, most notably water, ammonia, and methane ice. However, due to its very high element abundance, its degree of condensation never exceeds 0.2 per cent.

Phosphorus is the only element that has a distinctly non-monotonic degree of condensation. With increasing distance, it condenses out close to 1 au, returns to the gas phase near 3 au, and finally condenses out again at $r > 200$ au.

Even though many refractory elements are almost completely bound in condensates from the inner to the outer regions of the disc, the actual condensates formed by them change with distance. Since many of the elements are found in multiple different condensates, they all compete with each other for the available elements. This is illustrated for a sample of magnesium-, aluminum-, and titanium-bearing condensates in the upper panel of Fig. 6.

With increasing distance from the disc's centre, magnesium first condenses out into enstatite, forsterite, and spinel. Up to distances of 3 au, enstatite and forsterite compete for being the highest abundance magnesium-bearing condensate. At 3 au, $Mg(OH)_2$ forms and takes up most of the available magnesium. Consequently, forsterite is no longer able to exist, while enstatite is still able to co-exist as it requires smaller amounts of magnesium to form.

Aluminum is first found predominantly in the form of spinel ($MgAl_2O_4$). Near 0.5 au, it competes with $NaAlSi_3O_8$ for the element silicon and finally disappears close to 2 au in favour of corundum (Al_2O_3). The latter, though, is only stable for a short range of distances and is then replaced by Al_2SiO_5. This species can easily form there because the disappearance of forsterite in favour of $Mg(OH)_2$ provides an abundant amount of silicon. As more silicon becomes available, the abundance of corundum is decreased again by the formation of $NaAlSi_3O_8$, but still remains stable.

Titanium is predominantly found in only two condensates: TiO_2 and $MgTiO_3$. Unlike magnesium or aluminum, it does apparently not form several different condensates simultaneously. The innermost stable Ti-compound is TiO_2. It is replaced by $MgTiO_3$ near 1 au. However, with the formation of $Mg(OH)_2$ not enough magnesium is left and titanium returns to form TiO_2.

As shown in the bottom panel of Fig. 6, at lower temperatures the volatile species H_2O, CH_4, and NH_3 condense beyond 3, 4, and 70 au, respectively. These condensing species effectively remove the elements O, C, and N from the gas phase. The last element to leave the gas phase is phosphorus. As already noted above, P has a non-monotonic degree of condensation. Near 1 au, it first condenses out into $Mg_3P_2O_8$. With the formation of $Mg(OH)_2$, though, magnesium

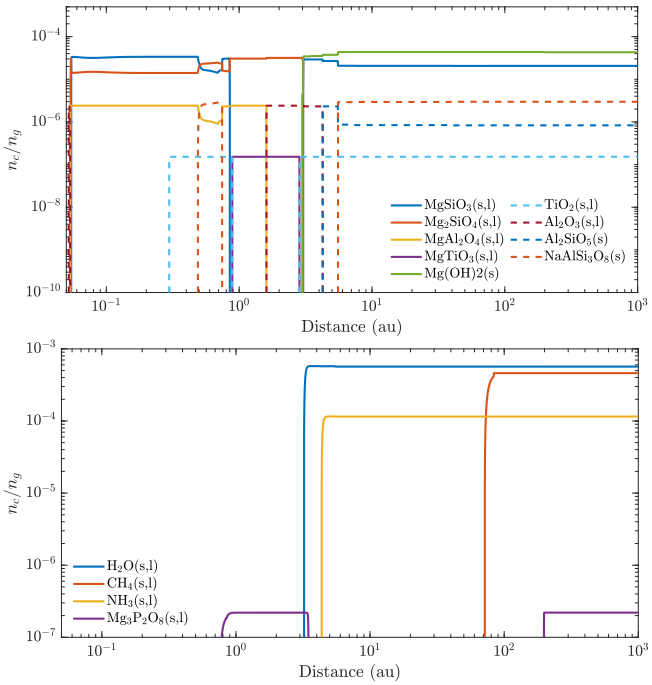

Figure 6. Abundance profiles of selected condensates as a function of distance in the protoplanetary disc model. The upper panel focuses on Mg-, Ti-, and Al-bearing refractory condensates, while the lower panel shows the more volatile condensate species.

is no longer available. Since also no other phosphorus-bearing condensate has a high enough activity, phosphorus returns back to the gas phase. Only at much lower temperatures in the outer part of the disc, some magnesium becomes available again to form $Mg_3P_2O_8$, removing P from the gas phase once more.

As discussed in Section 2.3, the phase rule and the requirement that the resulting system of activity equations for the set of stable condensates needs to be linearly independent limit the number of stable condensates. The latter requirement, however, also suggests that each condensed species should be linked with a related element that is associated with its stability. Often, this should be the least abundant element contained in a condensate normalized with the corresponding stoichiometric coefficient (see also Appendix B).

To illustrate this, we focus on the condensates present at the outermost grid point of the protoplanetary disc. According to Fig. 5, this point has the highest possible number of elements contained in condensates. All other elements left in the gas phase are the noble gases (He, Ne, and Ar) that do not have any condensate species associated with them in FASTCHEM COND. In Table 1, we list all 22 condensate species that are stable in the outer part of the disc. We also list the associated element for each condensate and the fraction of the fictitious condensate density n_c and its largest possible value $n_{c,\max}$ (see equation 13). If n_c is smaller than $n_{c,\max}$, the linked element is contained in more than one condensate. The assignment of the condensates to their respective elements is done by the procedure described in Appendix B.

The table clearly suggests that each element is uniquely linked with one specific condensate. Even though some elements, such as Mg or Al, can form several different condensates simultaneously, they are the associated species in only a single condensate. In many cases, the associated element is also the least abundant one in a specific condensate, often containing the total available inventory

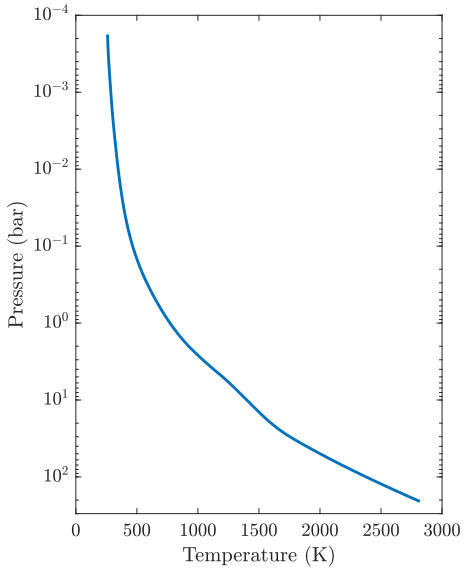

Figure 7. Temperature–pressure profile of a typical T5 brown dwarf used for the chemistry calculations. The profile is taken from the grid of Marley et al. (2021) for an effective temperature of 750 K and a surface gravity of $g = 3.16 \times 10^4$ cm s^{-2} ($\log g = 4.5$).

of that element. This also explains why, for example, the titanium-bearing condensates form very distinct condensation sequences (see Figs 3 and 6). Species like TiO_2(s, l), Ti_2O5(s, l), or $MgTiO_3$(s, l) cannot exist simultaneously as Ti would be the associated and least abundant element in all of them. Magnesium, on the other hand, can also be present in other condensate species besides $Mg(OH)_2$(s), such as $MgSiO_3$(s, l) in this example here, because it cannot fully condense out in a single condensate due to its higher abundance compared to the other elements in these condensates. Thus, elements with higher element abundances will usually tend to form multiple different condensates if those also contain elements with smaller abundances.

4.3 Equilibrium condensation versus rainout approximation

Finally, we apply the FASTCHEM code to an atmosphere of a typical brown dwarf. As discussed in Section 3.6, for atmospheres of planets and brown dwarfs the rainout approximation is a more suitable approach to calculate the chemical composition than the pure equilibrium condensation used in the previous two examples. In the following, we will show the impact of these two different approaches on the forming condensates and the chemical species remaining in the gas phase.

For the atmospheric temperature–pressure structure of the brown dwarf, we use output from the `Sonora` grid of brown dwarf models published by Marley et al. (2021), available on Zenodo.[4] In particular, we choose a model with an effective temperature of 750 K and a surface gravity of $g = 3.16 \times 10^4$ cm s^{-2} ($\log g = 4.5$), resembling a typical T5 dwarf. The corresponding temperature–pressure profile is shown in Fig. 7. Based on the general understanding of brown dwarf atmospheres, we expect the lower atmosphere to be dominated by the condensation of iron and various silicates, while in the upper atmosphere species like Na_2S, NaCl, or KCl should appear (see Morley et al. 2012; Marley et al. 2013, for example).

[4]https://zenodo.org/record/5063476

The temperature–pressure profile is used as an input for two different chemistry calculations with FASTCHEM COND, the first one using the standard equilibrium condensation approach from the two previous test cases and a second case with the rainout approximation. As described in Section 3.6, for the latter one we start the chemistry calculations at the bottom of the atmosphere and proceed upwards towards lower pressure, while calculating the gas phase composition and the condensed phase, respectively. Once condensation is encountered, we use the resulting fictitious number densities n_c of the condensates to calculate the effective abundances ϕ_j of these elements left in the gas phase. These new, reduced element abundances are then used in the subsequent calculations of the upper atmosphere.

In the top panel of Fig. 8, we show some important iron-, calcium-, and magnesium-bearing condensates comparing both condensation descriptions. Iron is one of the first condensates to become stable at a pressure of roughly 70 bar and a temperature of about 2200 K. Above this pressure, no condensate currently included in FASTCHEM COND can stably exist because of the high temperatures at the bottom of the atmosphere. For the equilibrium condensation, iron is found in the form of Fe(s, l) in the lower atmosphere, while in the upper atmosphere the dominant iron-bearing condensates are fayalite [Fe_2SiO_4(s)], magnetite [Fe_3O_4(s)], and FeS(s).

In contrast to that, the condensation into Fe(s, l) at pressures of about 10 bar already depletes the gas phase iron element abundance in the upper atmosphere for the rainout approximation. Consequently, no other Fe compounds can form there as essentially no iron is left in the gas phase at pressures lower than about 4 bar. The rainout of iron into an Fe(s, l) condensate layer and, consequently, its absence in the upper atmosphere agrees with results previously described in studies such as Marley et al. (2021) or Visscher, Lodders & Fegley (2010).

The corresponding results for major calcium- and magnesium-bearing condensates are depicted in the top middle panel of Fig. 8. Here, we can clearly see that in the equilibrium condensation case, calcium is first condensed in $CaTiO_3$(s) as well as Ca_2SiO_4(s). Around 20 bar, Ca is briefly mostly contained in $CaSiO_3$(s), while the upper atmosphere is then dominated by $CaMgSi_2O_6$(s).

The latter two condensates do not form in the rainout approach, however. Here, Ca is depleted in the lower atmosphere by condensation into $CaTiO_3$(s) and Ca_2SiO_4(s). As a result, more complex, secondary condensates like $CaMgSi_2O_6$(s) cannot form in the upper atmosphere.

Magnesium is mostly contained in the two condensates: forsterite [Mg_2SiO_4(s, l)] and enstatite [$MgSiO_3$(s, l)]. Condensation of forsterite takes place at pressures below the 20 bar level in the equilibrium condensation calculation, followed by $MgSiO_3$(s, l) between 10 and 0.1 bar. Both condensates co-exist in this pressure range, competing both for the available magnesium. Below pressures of 0.1 bar, however, $MgSiO_3$(s, l) stops forming, while forsterite becomes the dominating magnesium-bearing condensate. The second-most abundant magnesium condensate assuming the equilibrium condensation approach in the upper atmosphere is Mg_3P2O_8(s, l).

In the rainout approach, on the other hand, enstatite does not form. Condensation of magnesium into forsterite near 20 bar already depletes the gas phase of magnesium in the upper atmosphere, such that $MgSiO_3$(s, l) as well as other Mg-bearing species are unable to form.

The top right panel of Fig. 8 shows the condensation of sodium- and potassium-bearing species. In the equilibrium condensation calculation, Na first condenses into albite [$NaAlSi3O_8$(s)] near a

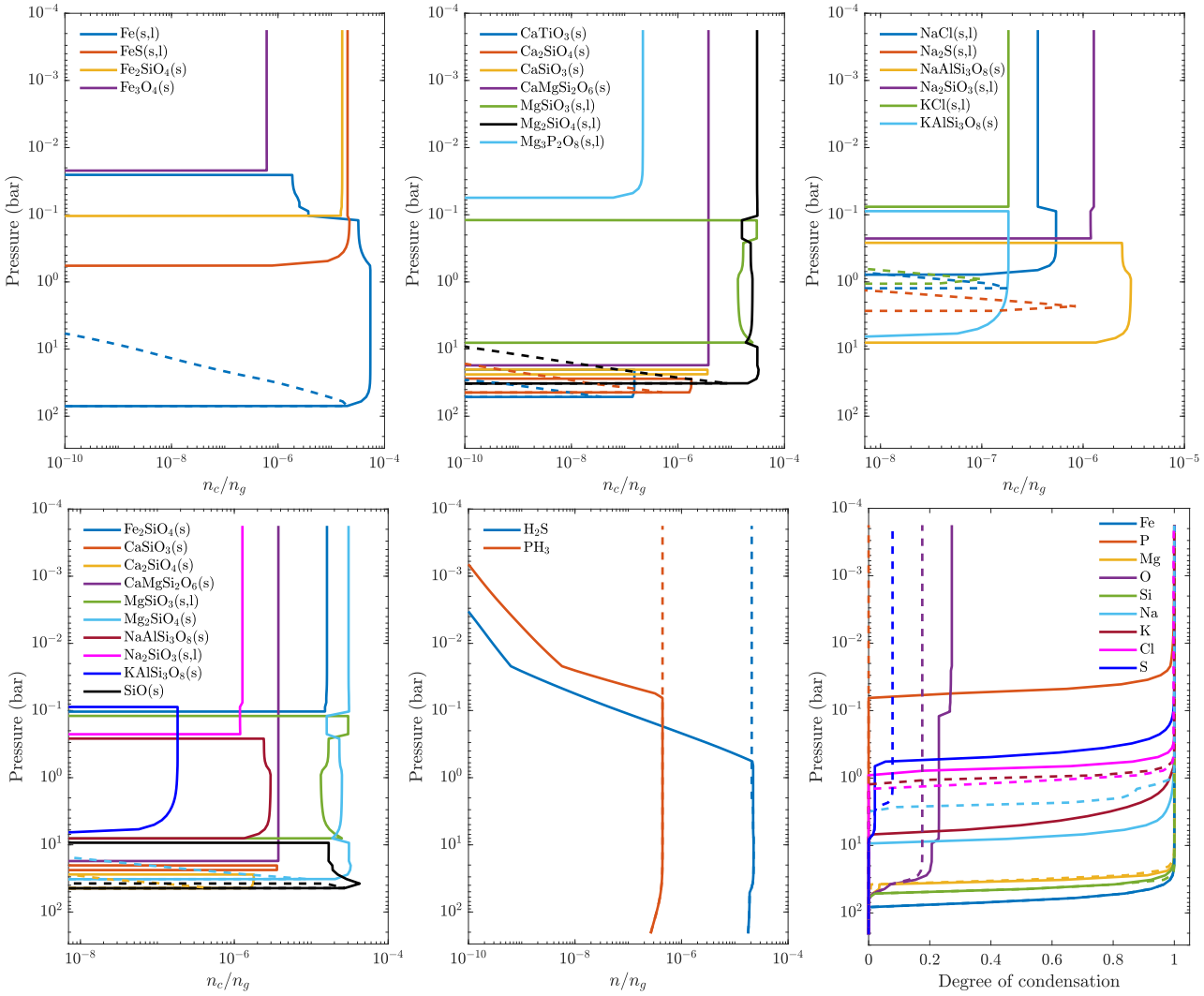

Figure 8. Impact of condensation on the chemistry of a brown dwarf atmosphere. The top panel shows abundance profiles for selected condensates: iron-bearing condensates (left), magnesium and calcium species (middle), and sodium and potassium condensates (right). Bottom panel: abundance profiles for silicon-bearing condensates (left), impact of the two different condensation approaches on the two gas phase species, namely hydrogen sulfide (H_2S) and phosphine (PH_3) (middle), and the degree of condensation for selected elements (right). The solid lines refer to the equilibrium condensation calculations. Dashed lines indicate the results for the rainout approximation.

pressure of 9 bar and into halite [NaCl(s)] below 1 bar. Around 0.2 bar, albite is replaced by sodium silicate [Na_2SiO_3(s, l)] as the most abundant sodium-bearing condensate. Potassium is only found in two stable condensates: microcline [$KAlSi_3O_8$(s)] in the lower atmosphere and KCl(s) (sylvite) in the upper part.

In the rainout approach model, albite is unable to form because neither silicon nor aluminum is available as they have already been depleted in the deeper atmosphere. Consequently, sodium stays in the gas phase at lower pressures compared to the equilibrium condensation case and finally condenses out into Na_2S at about 3 bar and NaCl near 1 bar. At roughly the same pressure level, potassium rains out into a sylvite layer without forming an additional condensate species.

The condensation sequence of silicon-bearing species is depicted in the bottom left panel of Fig. 8. As the figure suggests, this sequence is rather complicated, with silicon being present in as many as five different condensates simultaneously. In the lower atmosphere, Si is mostly contained in Ca-bearing condensates and SiO(s) whereas in the upper atmosphere it is predominantly chemically bound in forsterite, fayalite, diopside, and Na_2SiO_3(s, l). The absence of quartz [SiO_2(s)] as a stable condensate in the equilibrium condensation approach is consistent with studies such as Visscher et al. (2010), though it has been predicted to form under non-equilibrium conditions (Helling & Woitke 2006). In the rainout approximation, silicon rains out already in the deeper atmosphere into three distinct condensates: SiO(s), larnite [Ca_2SiO_4(s)], and forsterite.

The two different condensation treatments do have an impact not only on the condensing species, but also on the chemical composition of the gas phase. Examples for two gas phase molecules are shown in the bottom middle panel of Fig. 8. The most well-known example is the impact on H_2S, as already extensively discussed in the literature (see Lodders & Fegley 2002, for example). As already discussed, in the equilibrium condensation approach, iron is mostly contained in FeS(s, l) in the upper atmosphere, depleting the gas phase of both iron and sulphur. As a result, the H_2S molecule is unable to efficiently form in the gas phase in the upper atmosphere.

In contrast to the equilibrium condensation approach, we can see that H_2S is abundantly present in case of the rainout approximation. This is caused by the aforementioned depletion of iron into Fe(s, l) in the lower atmosphere. As a result, FeS(s, l) is unable to form in the rainout case and sulphur remains available to form H_2S.

Another gas phase species strongly affected by the differences of the two condensation treatments is phosphine (PH_3) as suggested by the results shown in Fig. 8. In the equilibrium condensation approach, phosphorus condenses into $Mg_3P_2O_8$(s, l) in the upper atmosphere, as depicted in Fig. 8. However, this condensate cannot be formed in the calculation with the rainout approximation because Mg is removed from the gas phase in the deeper atmosphere. Consequently, enough phosphorus remains in the gas phase to form phosphine.

The impact of the two different condensation descriptions can also seen in the form of the element depletion, depicted in the bottom right panel of Fig. 8. While the degree of condensation for elements in high-temperature condensates, such as Fe, Si, or Mg, is not strongly affected by the condensation treatment, larger differences can be noted in the aforementioned elements S and P. For the equilibrium condensation approach, both condense out at 1 bar and about 0.1 bar, respectively. In the rainout scenario, however, only about 10 per cent of sulphur actually condenses into Na_2S(s, l), while the degree of condensation for phosphorous remains zero throughout the entire atmosphere. Other elements, such as sodium or potassium, condense out completely in both condensation approaches, albeit they leave the gas phase at considerable lower pressures for the rainout approximation. Conversely, chlorine already rains out at higher pressures than in the equilibrium condensation calculation.

5 SUMMARY

In this study, we introduce a new version of FASTCHEM. With a version number of 3.0, we refer to this updated code as FASTCHEM COND. While the two previous versions of FASTCHEM only accounted for the gas phase composition, the new version now introduces the treatment of condensates to the code. In particular, FASTCHEM COND can compute scenarios involving equilibrium condensation as well as the rainout approximation often used in the modelling of atmospheres of (exo)planets and brown dwarfs. Together with the code update, we also add about 290 liquid and solid condensate species to FASTCHEM.

The numerical treatment of condensates is based on the basic ideas presented by Leal et al. (2016) and has been successfully adapted to the numerical formalism used in FASTCHEM. A major advantage compared to other established equilibrium condensation codes in the field of astrophysics is the automatic selection of stable condensates satisfying the phase rule.

The updated version of FASTCHEM is tested for several scenarios involving condensation. In particular, we reproduce the equilibrium condensation calculations by Sharp & Huebner (1990) and also test FASTCHEM COND for the numerically very challenging scenario of the mid-plane of a protoplanetary disc. Finally, we use a theoretical atmosphere model of a typical T5 brown dwarf to showcase the differences between equilibrium condensation and the rainout approximation.

FASTCHEM COND is programmed in object-oriented C++ and offers the additional PYTHON module PYFASTCHEM that allows it to be run directly from any PYTHON script. The code is released as open source at GitHub (https://github.com/exoclime/FastChem) under the GNU General Public License version 3 (gnu.org 2007). The repository also contains several PYTHON example scripts that showcase the use of FASTCHEM COND under PYTHON, as well as an extensive manual that provides detailed descriptions of the code, its required inputs, and available optional parameters.

ACKNOWLEDGEMENTS

The authors would like to dedicate this publication to the memory of Erwin Sedlmayr who passed away in 2022 January. DK acknowledges financial support from the Center for Space and Habitability (CSH) of the University of Bern. This work has been carried out within the framework of the NCCR PlanetS supported by the Swiss National Science Foundation under grants 51NF40_182901 and 51NF40_205606. DK would like to thank Jesse Weder and Christoph Mordasini for providing the temperature–pressure structure of the protoplanetary disc used in this study.

DATA AVAILABILITY

The data underlying this paper are available in the FASTCHEM GitHub repository, at https://github.com/exoclime/FastChem.

REFERENCES

Ackerman A. S., Marley M. S., 2001, ApJ, 556, 872
Asplund M., Grevesse N., Sauval A. J., Scott P., 2009, ARA&A, 47, 481
Barin I., 1995, Thermochemical Data of Pure Substances. VCH, Weinheim
Besmann T. M., 1977, Technical Report ORNL/TM-5775, SOLGASMIX-PV, a Computer Program to Calculate Equilibrium Relationships in Complex Chemical Systems. Oak Ridge National Laboratory, Oak Ridge, TN
Brinkley S. R.,, Jr, 1946, J. Chem. Phys., 14, 563
Brinkley S. R.,, Jr, 1947, J. Chem. Phys., 15, 107
Burrows A., Sharp C. M., 1999, ApJ, 512, 843
Cameron A. G. W., 1973, Space Sci. Rev., 15, 121
Chase M., 1998, NIST-JANAF Thermochemical Tables. Am. Inst. Phys., New York
Denbigh K., 1955, The Principles of Chemical Equilibrium. Cambridge Univ. Press, Cambridge
Dennis J. E.,, Jr, Schnabel R. B., 1996, Classics in Applied Mathematics, Numerical Methods for Unconstrained Optimization and Nonlinear Equations. Society for Industrial and Applied Mathematics, Philadelphia, PA
Deuflhard P., 2011, Newton Methods for Nonlinear Problems: Affine Invariance and Adaptive Algorithms. Springer-Verlag, Berlin
Dykyj J., Svoboda J., Wilhoit R. C., Frenkel M., Hall K. R., 2001, Landolt-Börnstein – Group IV Physical Chemistry, Volume 20C, Vapor Pressure and Antoine Constants for Nitrogen Containing Organic Compounds. Springer-Verlag, Berlin
Ebel D. S., 2006, in Lauretta D. S., McSween H. Y.,, Jr, eds, Meteorites and the Early Solar System II. Univ. Arizona Press, Tucson, AZ, p. 253
Ebel D. S., 2021, Condensation Calculations in Planetary Science and Cosmochemistry, available at https://oxfordre.com/planetaryscience/view/10.1093/acrefore/9780190647926.001.0001/acrefore-9780190647926-e-201
Emsenhuber A., Mordasini C., Burn R., Alibert Y., Benz W., Asphaug E., 2021, A&A, 656, A69
Eriksson G., 1971, Acta Chem. Scand., 25, 2651
Eriksson G., 1975, Chem. Scr., 8, 100
Fegley B., Palme H., 1985, Earth Planet. Sci. Lett., 72, 311
Gail H.-P., Sedlmayr E., 2013, Physics and Chemistry of Circumstellar Dust Shells. Cambridge Univ. Press, Cambridge
Gail H. P., Wetzel S., Pucci A., Tamanai A., 2013, A&A, 555, A119
Gao P., Wakeford H. R., Moran S. E., Parmentier V., 2021, J. Geophys. Res. (Planets), 126, e06655
Gibbs J. W., 1876, Trans. Connecticut Acad. Arts Sci., 3, 108
Gibbs J. W., 1878, Trans. Connecticut Acad. Arts Sci., 3, 343
gnu.org, 2007, GNU General Public License, available at: https://www.gnu.org/licenses/gpl-3.0.en.html [Access September 2023]
Goodwin R. D., 1985, J. Phys. Chem. Ref. Data, 14, 849

Gordon S., McBride B., 1994, Technical Report NASA RP-1311, Computer Program for Calculation of Complex Chemical Equilibrium Compositions and Applications. NASA, Washington, DC
Haar L., Gallagher J. S., 1978, J. Phys. Chem. Ref. Data, 7, 635
Helling C., Woitke P., 2006, A&A, 455, 325
Henning T., Semenov D., 2013, Chem. Rev., 113, 9016
Hoefner S., Jorgensen U. G., Loidl R., Aringer B., 1998, A&A, 340, 497
Huff V. N., Gordon S., Morrell V. E., 1951, Technical Report NACA-TR-1037, General Method and Thermodynamic Tables for Computation of Equilibrium Composition and Temperature of Chemical Reactions. NASA, Washington, DC
Kitzmann D., Patzer A. B. C., von Paris P., Godolt M., Rauer H., 2011, A&A, 531, A62
Kulik D., Wagner T., Dmytrieva S., Kosakowski G., Hingerl F., Chudnenko K., Berner U., 2013, Comput. Geosci., 17, 1
Leal A. M. M., Kulik D. A., Kosakowski G., Saar M. O., 2016, Adv. Water Resour., 96, 405
Lee E., Dobbs-Dixon I., Helling C., Bognar K., Woitke P., 2016, A&A, 594, A48
Lide D., 2009, CRC Handbook of Chemistry and Physics, 90th edn. CRC Press, Boca Raton, FL
Lodders K., Fegley B., 1993, Earth Planet. Sci. Lett., 117, 125
Lodders K., Fegley B., 1997, in Bernatowicz T. J., Zinner E., eds, AIP Conf. Proc. Vol. 402, Astrophysical Implications of the Laboratory Study of Presolar Materials. Am. Inst. Phys., New York, p. 391
Lodders K., Fegley B., 2002, Icarus, 155, 393
Marley M. S., Ackerman A. S., Cuzzi J. N., Kitzmann D., 2013, in Mackwell S. J., Simon-Miller A. A., Harder J. W., Bullock M. A., eds, Comparative Climatology of Terrestrial Planets. Univ. Arizona Press, Tucson, AZ, p. 367
Marley M. S. et al., 2021, ApJ, 920, 85
McBride B. J., Gordon S., 1996, Technical Report NASA RP-1311-P2, Computer Program for Calculation of Complex Chemical Equilibrium Compositions and Applications: II. Users Manual and Program Description. NASA Glenn Research Center, Cleveland, OH
McBride B., Zehe M., Gordon S., 2002, Technical Report NASA TP-2002-211556, NASA Glenn Coefficients for Calculating Thermodynamic Properties of Individual Species. NASA Glenn Research Center, Cleveland, OH
Morley C. V., Fortney J. J., Marley M. S., Visscher C., Saumon D., Leggett S. K., 2012, ApJ, 756, 172
Moses J. I., Allen M., Yung Y. L., 1992, Icarus, 99, 318
Murphy D. M., Koop T., 2005, Q. J. R. Meteorol. Soc., 131, 1539
Palme H., Fegley B.,, Jr, 1990, Earth Planet. Sci. Lett., 101, 180
Prydz R., Goodwin R. D., 1972, J. Chem. Thermodyn., 4, 127
Reynolds W. C., 1986, Technical Report, The Element-Potential Method for Chemical Equilibrium Analysis: Implementation in the Interactive Program STANJAN. Stanford University, Stanford, CA
Sharp C. M., Huebner W. F., 1990, ApJS, 72, 417
Smith W., Missen R., 1982, Chemical Reaction Equilibrium Analysis: Theory and Algorithms. Wiley, New York
Stock J. W., Kitzmann D., Patzer A. B. C., Sedlmayr E., 2018, MNRAS, 479, 865
Stock J. W., Kitzmann D., Patzer A. B. C., 2022, MNRAS, 517, 4070
van Zeggeren F., Storey S., 1970, The Computation of Chemical Equilibria. Cambridge Univ. Press, Cambridge
Visscher C., Fegley B.,, Jr, 2005, ApJ, 623, 1221
Visscher C., Lodders K., Fegley B.,, Jr, 2010, ApJ, 716, 1060
Wagner W., Kretzschmar H.-J., 2008, International Steam Tables: Properties of Water and Steam Based on the Industrial Formulation IAPWS-IF97. Springer-Verlag, Berlin
Weder J., Mordasini C., Emsenhuber A., 2023, A&A, 674, A165
White W. B., Johnson S. M., Dantzig G. B., 1957, Technical Report P-1059, Chemical Equilibrium in Complex Mixtures. RAND Corp., Santa Monica, California
White W. B., Johnson S. M., Dantzig G. B., 1958, J. Chem. Phys., 28, 751
Winters J. M., Le Bertre T., Jeong K. S., Helling C., Sedlmayr E., 2000, A&A, 361, 641
Woitke P., Helling C., Hunter G. H., Millard J. D., Turner G. E., Worters M., Blecic J., Stock J. W., 2018, A&A, 614, A1
Yaws C. L., 1999, Chemical Properties Handbook: Physical, Thermodynamic, Environmental, Transport, Safety, and Health Related Properties for Organic and Inorganic Chemicals. McGraw-Hill, New York
Zeleznik F. J., Gordon S., 1960, Technical Report NASA-TN-D-473, An Analytical Investigation of Three General Methods of Calculating Chemical-Equilibrium Compositions. NASA, Washington, DC
Zeleznik F. J., Gordon S., 1968, Ind. Eng. Chem., 60, 27

APPENDIX A: DATA FITS

The calculation of the condensed phase requires some important thermochemical data as basic input, namely the temperature-dependent equilibrium constants. The dimensionless equilibrium constant $\bar{K}_c(T)$ for a specific condensate c is calculated from the Gibbs free energy of reaction (e.g. Stock et al. 2018):

$$\ln \bar{K}_c(T) = -\frac{\Delta_r G_c^{\ominus}(T)}{RT} , \tag{A1}$$

where $\Delta_r G_c^{\ominus}$ is the change of Gibbs free energy for the dissociation reaction

$$\mathrm{A_aB_bC_c(s)} \rightleftharpoons \mathrm{aA(g) + bB(g) + cC(g)} , \tag{A2}$$

of a condensate species into its elements, given by

$$\begin{aligned}\Delta_r G_c^{\ominus}(T) &= \Delta_f G_c^{\ominus}(T) - \sum_{j\in\mathcal{E}} \nu_{cj} \Delta_f G_j^{\ominus}(T) \\ &= G_c^{\ominus}(T) - \sum_{j\in\mathcal{E}} \nu_{cj} G_j^{\ominus}(T) , \qquad c \in \mathcal{C} .\end{aligned} \tag{A3}$$

Here, the $\Delta_f G_c^{\ominus}(T)$ are the Gibbs free energies of formation and the $G_c^{\ominus}(T)$ the corresponding Gibbs free energies. It is important to note that the tabulated thermochemical data, such as the $\Delta_f G^{\ominus}(T)$ or the $\ln \bar{K}$, in the corresponding data bases are always given with respect to the elements in a specific reference state. For example, the JANAF tables (Chase 1998) use in general the chemically most stable form of an element at standard pressure and a temperature of 298.15 K as the reference state. Thus, the thermochemical data of, for example, CO_2 is given with respect to C(s) and O_2 in the JANAF tables because the stable form of oxygen at 1 bar and 298.15 K is molecular oxygen while carbon's is graphite. By calculating the equilibrium constants via equations (A1) and (A3) with FASTCHEM, we effectively adjust the reference state of the elements from the tabulated data to their monatomic form. Thus, the $\ln \bar{K}$ used in FASTCHEM and given in Table A1 should not be confused with the corresponding $\ln \bar{K}$ tabulated in thermochemical data bases, such as the JANAF tables. Data from different sources therefore generally cannot be used interchangeably with FASTCHEM and usually need to be converted to the reference state used in our formalism.

If the number densities n_j are given in units of $\mathrm{cm^{-3}}$, then in the activity equation (14) for the condensates K_c has units of

$$[K_c] = \left(\mathrm{cm^{-3}}\right)^{-\sum_{j\in\mathcal{E}} \nu_{cj}} . \tag{A4}$$

It is related to the dimensionless mass action constant $\bar{K}_c(T)$ by

$$\ln K_c(T) = \ln \bar{K}_c(T) - \ln\left(\frac{p^{\ominus}}{k_B T} \sum_{j\in\mathcal{E}} \nu_{cj}\right) , \tag{A5}$$

where $p^{\ominus}$ is the pressure of the standard state of the thermochemical data. We note that this relation explicitly makes use of the ideal gas law. For the data used in the FASTCHEM code, $p^{\ominus}$ is equal to 1 bar.

Table A1. An overview of condensates and the fit coefficients for the equilibrium constants included in FASTCHEM. Species with both liquid and solid phases have two separate sets of coefficients. The first line always refers to the solid species, while the second line represents the liquid phase. It is important to note that the tabulated $\ln \bar{K}$ use the elements in their monatomic form as reference state (see text for details).

Species	Name	a_0	a_1	b_0	b_1	b_2	References
Al(s)	Aluminum	3.956 147e+04	− 8.786 728e−01	−1.167 603e+01	2.133 162e−03	− 3.413 406e−07	1
Al_2O_3(s, l)	Corundum	3.684 822e+05	− 1.041 942e+01	−2.792 435e+01	1.179 042e−02	− 1.587 869e−06	1
	Aluminum oxide	3.713 491e+05	5.273 685e+00	−1.353 453e+02	1.681 739e−03	− 8.802 596e−08	
Al_2S_3(s)	Aluminum sulfide	2.563 027e+05	− 7.095 578e+00	−4.462 246e+01	1.119 856e−02	− 1.975 854e−06	1
Al_2SiO_5(s)	Aluminum silicate, kyanite	5.918 298e+05	− 1.467 960e+01	−5.539 231e+01	1.428 258e−02	− 1.532 276e−06	1
Al_4C_3(s)	Aluminum carbide	4.407 611e+05	− 1.036 553e+01	−6.167 107e+01	1.118 864e−02	− 1.248 269e−06	1
$Al_6Si_2O_{13}$(s)	Aluminum silicate, mullite	1.547 250e+06	− 3.695 282e+01	−1.487 433e+02	3.637 935e−02	− 4.036 965e−06	1
$AlCl_3$(s, l)	Aluminum chloride	1.675 202e+05	− 7.550 810e+00	−2.652 395e+01	2.274 542e−02	− 1.018 958e−05	1
		1.652 902e+05	2.464 703e+00	−7.571 900e+01	1.931 285e−03	− 2.825 885e−07	
AlClO(s)	Aluminum chloride oxide	1.794 890e+05	− 1.203 782e+00	−4.577 195e+01	2.044 840e−03	− 1.880 469e−07	1
AlF_3(s, l)	Aluminum fluoride	2.487 414e+05	− 5.745 158e+00	−3.427 156e+01	7.085 042e−03	− 9.144 723e−07	1
		2.360 574e+05	− 3.743 293e+00	−3.872 272e+01	2.682 689e−03	− 1.350 757e−07	
AlN(s)	Aluminum nitride	1.339 375e+05	− 3.463 105e+00	−1.434 411e+01	3.453 076e−03	− 3.929 430e−07	1
C(s)	Graphite	8.568 812e+04	− 1.859 707e+00	−6.365 415e+00	1.052 982e−03	− 6.538 803e−08	1
CH_4(s, l)	Methane	1.988 879e+05	− 2.100 289e+00	−3.215 642e+01	− 5.115 678e−02	4.954 560e−05	2
		1.993 153e+05	1.153 444e+01	−8.945 224e+01	− 1.628 836e−01	2.023 426e−04	
CO(l)	Carbon monoxide	1.298 145e+05	2.919 441e+00	−3.273 636e+01	− 1.572 012e−02	− 5.510 555e−05	3
CO_2(s, l)	Carbon dioxide	1.991 499e+05	1.438 951e+02	−5.973 862e+02	− 1.693 532e+00	2.816 767e−03	4
		2.008 946e+05	6.846 712e+01	−3.867 496e+02	− 2.638 778e−01	1.596 368e−04	
$Ca(OH)_2$(s)	Calcium hydroxide	2.504 859e+05	− 1.074 866e+01	−1.225 092e+01	1.759 083e−02	− 4.411 867e−06	1
Ca(s, l)	Calcium	2.149 529e+04	2.238 090e−01	−1.537 980e+01	2.557 372e−04	3.500 411e−07	1
		2.038 206e+04	6.678 459e−01	−1.739 738e+01	6.213 603e−04	− 6.114 669e−08	
$Ca_2Al_2SiO_7$(s)	Gehlenite	8.690 139e+05	− 8.773 045e−01	−2.108 860e+02	3.890 910e−03	− 1.420 233e−07	5
Ca_2SiO_4(s)	Larnite	4.938 758e+05	− 8.773 129e−01	−1.154 846e+02	2.596 067e−03	− 1.420 238e−07	5
$CaAl_2Si_2O_8$(s)	Anorthite	9.440 506e+05	− 1.961 755e+00	−2.236 517e+02	4.061 832e−03	− 1.246 940e−07	5
$CaCl_2$(s, l)	Calcium chloride	1.463 160e+05	− 7.420 422e−01	−4.262 592e+01	3.394 191e−03	− 8.074 484e−07	1
		1.451 897e+05	2.554 356e+00	−6.282 319e+01	1.077 119e−03	− 8.936 442e−08	
CaF_2(s, l)	Calcium fluoride	1.875 412e+05	− 2.241 695e+00	−3.559 303e+01	3.779 908e−03	− 2.709 703e−07	1
		1.848 023e+05	2.379 252e+00	−6.409 940e+01	9.778 805e−04	− 7.709 693e−08	
$CaMgSi_2O_6$(s)	Diopside	7.148 791e+05	− 2.026 835e+00	−1.670 276e+02	3.403 319e−03	− 1.557 866e−07	5
CaO(s, l)	Lime	1.274 223e+05	− 1.487 077e+00	−2.452 561e+01	2.263 440e−03	− 2.336 948e−07	1
	Calcium oxide	1.335 876e+05	1.154 889e+01	−1.210 960e+02	− 1.932 018e−03	4.857 311e−08	
CaS(s)	Calcium sulfide	1.115 334e+05	− 6.115 886e−01	−2.869 597e+01	1.525 313e−03	− 1.542 806e−07	1
$CaSiO_3$(s)	Wollastonite	3.627 167e+05	− 9.463 588e−01	−8.280 477e+01	1.787 685e−03	− 8.890 603e−08	5
$CaTiO_3$(s)	Perovskite	3.674 183e+05	− 1.766 903e−01	−8.730 090e+01	1.522 505e−03	− 6.177 887e−08	5
ClSSCl(l)	Sulfur chloride	1.039 544e+05	3.853 606e+00	−7.902 839e+01	2.217 898e−05	9.895 276e−08	1
Co(s, l)	Cobalt	5.131 664e+04	− 1.624 057e−01	−1.718 128e+01	4.248 043e−04	1.079 704e−07	1
		4.936 912e+04	4.397 571e−01	−2.021 232e+01	4.482 975e−04	− 2.596 585e−08	
Co_3O_4(s)	Cobalt oxide	3.805 484e+05	− 1.311 011e+01	−4.889 755e+01	1.492 909e−02	− 1.851 336e−06	1
$CoCl_2$(s, l)	Cobalt chloride	1.182 421e+05	− 3.463 875e−01	−4.766 135e+01	3.411 071e−03	− 9.200 809e−07	1
		1.126 187e+05	− 1.194 465e+00	−3.642 867e+01	2.978 683e−03	− 3.093 353e−07	
CoF_2(s, l)	Cobalt fluoride	1.506 989e+05	− 3.193 462e+00	−3.181 019e+01	6.137 417e−03	− 1.223 355e−06	1
		1.485 934e+05	4.552 908e+00	−8.005 494e+01	− 1.340 822e−04	1.341 266e−08	
CoF_3(s)	Cobalt fluoride	1.750 972e+05	− 1.031 290e−01	−6.748 535e+01	1.091 077e−03	− 6.583 164e−08	1
CoO(s)	Cobalt oxide	1.100 576e+05	5.701 443e−01	−3.845 427e+01	1.455 438e−04	5.439 530e−08	1
$CoSO_4$(s)	Cobalt sulfate	3.090 612e+05	− 1.116 262e+01	−3.771 972e+01	1.342 978e−02	− 1.891 004e−06	1
Cr(s, l)	Chromium	4.776 074e+04	− 4.402 638e−01	−1.579 587e+01	1.135 168e−03	− 5.798 430e−08	1
		4.812 046e+04	4.364 483e+00	−4.903 639e+01	− 8.052 095e−04	2.749 278e−08	
$Cr_{23}C_6$(s)	Chromium carbide	1.651 885e+06	− 2.815 593e+01	−3.629 898e+02	5.382 902e−02	− 7.115 388e−06	1
Cr_2N(s)	Chromium nitride	1.676 501e+05	− 3.745 241e−01	−5.139 066e+01	2.217 768e−03	− 1.117 960e−07	1
Cr_2O_3(s, l)	Chromium oxide	3.209 921e+05	− 4.756 124e+00	−6.173 275e+01	6.743 034e−03	− 8.731 748e−07	1
		3.151 896e+05	7.173 936e+00	−1.402 790e+02	− 5.100 608e−04	− 4.577 192e−09	
Cr_3C_2(s)	Chromium carbide	3.249 597e+05	− 5.902 197e+00	−5.588 923e+01	9.151 586e−03	− 1.088 919e−06	1
Cr_7C_3(s)	Chromium carbide	6.109 513e+05	− 9.093 707e+00	−1.268 842e+02	1.555 679e−02	− 1.704 735e−06	1
CrN(s)	Chromium nitride, carlsbergite	1.187 703e+05	− 4.973 699e−01	−3.255 611e+01	1.795 595e−03	− 2.412 700e−07	1
$Cu(OH)_2$(s)	Copper hydroxide	2.063 558e+05	− 3.959 163e+00	−4.948 256e+01	4.803 361e−03	− 6.293 209e−07	1
Cu(s, l)	Copper	4.063 664e+04	− 1.796 348e−01	−1.541 808e+01	1.094 894e−03	− 1.863 786e−07	1
		3.992 359e+04	1.143 037e+00	−2.354 187e+01	2.254 564e−04	− 2.859 314e−08	
Cu_2O(s, l)	Copper oxide	1.312 161e+05	− 2.985 239e+00	−3.107 042e+01	5.111 241e−03	− 8.064 332e−07	1
		9.760 053e+04	− 4.553 264e+01	2.730 661e+02	2.716 321e−02	− 2.449 896e−06	
CuCN(s)	Copper cyanide	1.716 651e+05	− 3.780 381e+00	−2.525 504e+01	7.348 382e−03	− 1.652 732e−06	1
CuCl(s, l)	Copper chloride	7.166 240e+04	− 2.279 191e+00	−1.794 801e+01	7.232 716e−03	− 1.983 595e−06	1
		7.164 885e+04	2.401 760e+00	−4.473 335e+01	3.431 803e−04	− 3.623 642e−08	
$CuCl_2$(s)	Copper chloride	9.455 309e+04	− 6.600 209e−01	−4.377 040e+01	2.643 987e−03	− 4.290 951e−07	1
CuF(s)	Copper fluoride	8.410 522e+04	2.339 656e−01	−3.397 521e+01	1.885 845e−03	− 2.357 838e−07	1

Table A1 – *continued*

Species	Name	a_0	a_1	b_0	b_1	b_2	References
CuF_2(s, l)	Copper fluoride	1.239 210e+05	− 4.086 542e+00	−2.582 427e+01	7.893 781e−03	− 1.490 332e−06	1
		1.201 494e+05	2.897 313e+00	−6.539 023e+01	9.315 675e−04	− 8.899 353e−08	
CuO(s)	Copper oxide	8.895 417e+04	− 2.221 543e+00	−2.134 043e+01	3.694 321e−03	− 5.357 891e−07	1
$CuSO_4$(s)	Copper sulfate	2.840 470e+05	− 1.142 242e+01	−3.544 105e+01	1.361 580e−02	− 1.928 828e−06	1
$Fe(CO)_5$(l)	Iron carbonyl	7.203 824e+05	− 3.761 358e+01	1.681 905e+01	1.282 803e−01	− 6.092 806e−05	1
$Fe(OH)_2$(s)	Iron hydroxide	2.304 052e+05	− 4.869 319e+00	−4.809 856e+01	5.794 217e−03	− 7.697 445e−07	1
$Fe(OH)_3$(s)	Iron hydroxide	3.161 186e+05	− 1.177 456e+01	−3.624 228e+01	1.140 455e−02	− 1.475 673e−06	1
Fe(s, l)	Iron	4.974 655e+04	− 1.591 894e+00	−9.409 153e+00	2.776 344e−03	− 2.676 971e−07	1
		5.079 703e+04	3.096 658e+00	−4.091 199e+01	− 4.838 448e−05	− 7.731 235e−09	
$Fe_2(SO_4)_3$(s)	Iron sulfate	8.653 884e+05	− 2.297 044e+01	−1.590 785e+02	2.277 154e−02	− 2.696 870e−06	1
Fe_2O_3(s)	Iron oxide, hematite	2.875 123e+05	− 8.618 740e+00	−4.016 576e+01	1.291 300e−02	− 1.814 306e−06	1
Fe_2SiO_4(s)	Fayalite	4.534 231e+05	− 1.015 392e+00	−1.192 593e+02	2.752 740e−03	− 3.578 755e−08	5
Fe_3O_4(s)	Iron oxide, magnetite	4.027 661e+05	− 9.466 152e+00	−6.950 241e+01	1.508 513e−02	− 1.944 451e−06	1
$FeCl_2$(s, l)	Iron chloride	1.203 448e+05	− 3.734 284e−01	−4.609 400e+01	2.428 654e−03	− 4.403 345e−07	1
		1.133 134e+05	− 5.693 037e+00	−6.086 630e+00	6.792 618e−03	− 7.496 602e−07	
$FeCl_3$(s, l)	Iron chloride	1.414 220e+05	− 3.683 131e+00	−4.480 520e+01	1.026 354e−02	− 3.135 510e−06	1
		1.360 565e+05	− 3.706 127e+00	−3.497 542e+01	8.553 835e−03	− 1.302 368e−06	
FeF_2(s, l)	Iron fluoride	1.533 412e+05	− 3.671 062e+00	−2.813 476e+01	6.031 207e−03	− 1.077 456e−06	1
		1.503 731e+05	2.114 308e+00	−6.271 308e+01	9.913 520e−04	− 8.604 572e−08	
FeF_3(s)	Iron fluoride	2.039 979e+05	6.578 156e−02	−6.800 792e+01	6.230 488e−04	6.927 721e−08	1
FeO(s, l)	Iron oxide	1.125 810e+05	− 8.222 241e−01	−2.941 345e+01	2.022 018e−03	− 2.157 028e−07	1
		1.125 140e+05	3.159 906e+00	−5.608 247e+01	− 8.454 633e−06	− 1.060 767e−08	
FeS(s, l)	Troilite	9.509 604e+04	− 4.082 122e+00	−1.321 710e+01	1.163 709e−02	− 2.944 081e−06	1
	Iron sulfide	9.213 673e+04	2.251 085e+00	−4.666 790e+01	9.905 113e−05	− 2.071 871e−08	
FeS_2(s)	Iron sulfide, pyrite	1.362 424e+05	− 5.216 929e+00	−2.472 416e+01	7.246 209e−03	− 1.224 809e−06	1
$FeSO_4$(s)	Iron sulfate	3.124 384e+05	− 1.174 652e+01	−3.362 834e+01	1.366 547e−02	− 1.903 293e−06	1
H_2O(s, l)	Water	1.161 044e+05	− 3.718 075e+00	−9.969 769e+00	− 3.487 074e−02	5.802 833e−05	6
		1.159 205e+05	− 1.223 011e+01	2.278 135e+01	4.478 035e−02	− 2.373 704e−05	
$H_2SO_4 \cdot 2\,H_2O$(s, l)	Sulfuric acid, dihydrate	5.421 586e+05	0.000 000e+00	−1.859 508e+02	0.000 000e+00	0.000 000e+00	1
		5.379 818e+05	− 2.361 357e+01	−4.825 948e+01	3.685 278e−02	− 4.514 038e−06	
$H_2SO_4 \cdot 3\,H_2O$(s, l)	Sulfuric acid, trihydrate	6.600 920e+05	0.000 000e+00	−2.255 215e+02	0.000 000e+00	0.000 000e+00	1
		6.553 913e+05	− 2.443 345e+01	−8.133 285e+01	3.702 767e−02	− 5.141 492e−06	
$H_2SO_4 \cdot 4\,H_2O$(s, l)	Sulfuric acid, tetrahydrate	7.776 671e+05	0.000 000e+00	−2.645 269e+02	0.000 000e+00	0.000 000e+00	1
		7.737 246e+05	− 1.921 562e+01	−1.506 327e+02	2.900 250e−02	− 3.713 059e−06	
$H_2SO_4 \cdot H_2O$(s, l)	Sulfuric acid, monohydrate	4.241 238e+05	0.000 000e+00	−1.476 872e+02	0.000 000e+00	0.000 000e+00	1
		4.207 448e+05	− 1.683 880e+01	−4.909 595e+01	2.826 498e−02	− 4.992 257e−06	
H_3PO_4(s, l)	Phosphoric acid	3.649 398e+05	− 3.610 999e+02	1.635 643e+03	1.659 642e+00	− 1.244 896e−03	1
		3.858 749e+05	− 1.943 246e+01	−5.302 719e+00	2.691 054e−02	− 2.100 131e−06	
$K(HF_2)$(s, l)	Potassium fluoride	1.686 015e+05	1.626 319e+01	−1.335 623e+02	− 8.347 054e−02	5.771 035e−05	1
		1.665 289e+05	8.874 422e−01	−6.179 823e+01	1.281 717e−03	− 1.627 841e−07	
K(s, l)	Potassium	1.077 119e+04	− 1.679 865e+00	−4.750 111e+00	1.105 795e−02	− 7.948 908e−06	1
		1.085 335e+04	1.658 842e+00	−2.136 304e+01	− 7.517 943e−04	1.673 343e−07	
K_2CO_3(s, l)	Potassium carbonate	3.343 443e+05	− 8.558 037e+00	−4.687 500e+01	1.286 535e−02	− 1.718 329e−06	1
		3.369 816e+05	4.157 171e+00	−1.297 355e+02	3.324 597e−03	− 3.044 607e−07	
K_2O(s)	Potassium oxide	9.572 263e+04	1.559 253e+00	−5.837 793e+01	2.141 865e−03	4.482 650e−08	1
K_2O_2(s)	Potassium peroxide	1.411 746e+05	− 7.040 524e−01	−6.172 071e+01	4.554 021e−03	− 1.252 715e−07	1
K_2S(s, l)	Potassium sulfide	1.018 381e+05	9.711 730e+00	−1.020 847e+02	− 1.591 247e−02	5.117 272e−06	1
		9.804 314e+04	2.913 293e+00	−6.343 656e+01	9.016 801e−04	− 8.185 043e−08	
K_2SO_4(s, l)	Potassium sulfate	3.454 310e+05	− 1.139 934e+01	−4.772 189e+01	1.574 027e−02	− 1.746 880e−06	1
		3.423 413e+05	5.296 285e−01	−1.169 303e+02	2.957 119e−03	− 2.371 220e−07	
K_2SiO_3(s, l)	Potassium silicate	3.498 376e+05	− 1.098 489e+01	−3.601 910e+01	1.887 993e−02	− 3.516 949e−06	1
		3.465 636e+05	2.172 528e+00	−1.115 910e+02	2.227 290e−03	− 1.900 013e−07	
$K_3Al_2Cl_9$(s)	Potassium aluminum chloride	5.873 654e+05	3.236 455e−02	−2.243 358e+02	7.124 397e−03	− 7.854 201e−08	1
K_3AlCl_6(s)	Potassium hexachloroaluminate	4.113 207e+05	− 7.415 459e−01	−1.509 520e+02	7.704 941e−03	− 6.003 396e−07	1
K_3AlF_6(s)	Potassium hexafluoraluminate	5.284 189e+05	− 5.965 318e+00	−1.253 129e+02	1.265 846e−02	− 1.322 514e−06	1
$KAlCl_4$(s)	Potassium tetrachloroaluminate	2.529 190e+05	− 1.016 468e+00	−9.212 325e+01	7.150 289e−03	− 6.981 276e−07	1
$KAlSi_3O_8$(s)	Microcline	9.255 717e+05	− 5.767 761e−10	−2.262 691e+02	3.706 558e−13	− 2.893 568e−17	5
KCN(s, l)	Potassium cyanide	1.686 987e+05	1.120 345e+01	−1.023 096e+02	− 2.744 777e−02	1.017 605e−05	1
		1.665 750e+05	1.215 299e+00	−4.869 149e+01	2.327 041e−04	− 2.641 994e−08	
KCl(s, l)	Sylvite	7.799 634e+04	2.164 702e−01	−3.146 200e+01	1.372 881e−03	− 1.226 827e−07	1
	Potassium chloride	7.532 773e+04	2.964 109e−02	−2.853 322e+01	2.400 027e−03	− 2.560 579e−07	
$KClO_4$(s)	Potassium perchlorate	1.941 104e+05	− 1.965 987e+01	1.221 054e+01	3.800 872e−02	− 7.788 120e−06	1
KF(s, l)	Potassium fluoride	8.861 397e+04	− 8.456 627e−01	−2.625 877e+01	2.808 236e−03	− 4.810 086e−07	1
		8.727 994e+04	2.303 486e+00	−4.537 539e+01	7.036 535e−04	− 6.149 724e−08	
KH(s)	Potassium hydride	4.356 033e+04	− 2.085 467e+00	−1.512 901e+01	3.606 523e−03	− 4.797 331e−07	1
KO_2(s)	Potassium superoxide	1.050 071e+05	− 7.728 754e−01	−4.074 377e+01	4.806 930e−03	− 8.106 701e−07	1

Table A1 – *continued*

Species	Name	a_0	a_1	b_0	b_1	b_2	References
KOH(s, l)	Potassium hydroxide	1.176 667e+05	− 4.819 711e−01	−3.767 670e+01	− 7.788 299e−03	9.191 450e−06	1
		1.164 340e+05	3.912 731e−01	−4.363 535e+01	1.633 090e−03	− 2.048 580e−07	
$Mg(OH)_2$(s)	Magnesium hydroxide	2.389 267e+05	− 1.292 321e+01	−5.297 023e−01	1.971 956e−02	− 4.788 722e−06	1
Mg(s, l)	Magnesium	1.770 507e+04	− 4.329 649e−01	−1.203 290e+01	1.820 868e−03	− 3.855 719e−07	1
		1.695 543e+04	2.988 436e−01	−1.560 396e+01	8.906 642e−04	− 9.747 666e−08	
Mg_2C_3(s)	Magnesium carbide	2.843 523e+05	− 1.188 247e+00	−7.453 823e+01	2.686 587e−03	− 2.338 453e−07	1
Mg_2Si(s, l)	Magnesium silicide	9.891 257e+04	− 6.845 227e−01	−4.322 943e+01	2.881 142e−03	− 3.449 654e−07	1
		9.100 387e+04	3.747 421e+00	−6.622 348e+01	3.256 929e−05	− 7.935 425e−09	
Mg_2SiO_4(s, l)	Forsterite	4.685 245e+05	− 1.260 765e+01	−4.533 909e+01	1.474 156e−02	− 2.019 847e−06	1
	Magnesium silicate	4.672 008e+05	3.105 344e+00	−1.454 310e+02	1.348 332e−03	− 8.110 942e−08	
Mg_2TiO_4(s, l)	Magnesium titanium oxide	4.700 251e+05	− 1.231 678e+01	−4.689 025e+01	1.565 454e−02	− 2.197 166e−06	1
		4.650 479e+05	6.163 277e+00	−1.646 344e+02	1.346 740e−03	− 1.018 401e−07	
Mg_3N_2(s)	Magnesium nitride	2.218 839e+05	− 2.274 009e+00	−6.695 963e+01	3.991 576e−03	− 5.068 377e−07	1
$Mg_3P_2O_8$(s, l)	Magnesium phosphate	8.208 372e+05	− 1.416 969e+01	−1.400 854e+02	1.687 648e−02	− 2.000 682e−06	1
		8.379 570e+05	2.081 898e+01	−3.891 739e+02	1.421 557e−03	− 1.122 682e−07	
$MgAl_2O_4$(s, l)	Spinel	4.905 698e+05	− 1.277 185e+01	−4.605 652e+01	1.415 049e−02	− 1.693 535e−06	1
	Magnesium aluminum oxide	4.747 388e+05	3.247 152e+00	−1.436 686e+02	1.810 017e−03	− 9.783 613e−08	
MgC_2(s)	Magnesium carbide	1.794 808e+05	− 7.146 464e−01	−4.564 324e+01	1.609 585e−03	− 1.397 661e−07	1
$MgCO_3$(s)	Magnesium carbonate	3.251 431e+05	− 1.244 718e+01	−1.310 458e+01	1.730 791e−02	− 3.510 841e−06	1
$MgCl_2$(s, l)	Magnesium chloride	1.238 737e+05	− 2.052 709e+00	−3.619 730e+01	5.877 005e−03	− 1.489 818e−06	1
		1.201 646e+05	1.847 462e+00	−5.572 742e+01	8.343 270e−04	− 7.266 538e−08	
MgF_2(s, l)	Magnesium fluoride	1.712 104e+05	− 4.591 530e+00	−2.243 934e+01	7.438 186e−03	− 1.344 173e−06	1
		1.650 826e+05	− 1.155 217e+00	−3.845 058e+01	2.240 213e−03	− 1.637 437e−07	
MgH_2(s)	Magnesium hydride	7.780 425e+04	− 6.636 259e+00	−7.191 223e−01	6.219 478e−03	− 8.158 665e−07	1
MgO(s, l)	Periclase	1.194 249e+05	− 2.372 738e+00	−1.943 966e+01	2.746 009e−03	− 2.913 453e−07	1
	Magnesium oxide	1.092 185e+05	− 2.366 847e+00	−1.431 364e+01	1.452 149e−03	− 6.711 535e−08	
MgS(s)	Magnesium Sulfide	9.243 983e+04	− 8.157 691e−01	−2.730 010e+01	1.496 078e−03	− 1.497 490e−07	1
$MgSO_4$(s, l)	Magnesium sulfate	3.200 432e+05	− 1.284 829e+01	−2.706 610e+01	1.567 552e−02	− 2.606 110e−06	1
		3.242 348e+05	3.274 547e+00	−1.304 625e+02	3.745 212e−04	− 2.944 070e−08	
$MgSiO_3$(s, l)	Enstatite	3.458 926e+05	− 1.021 310e+01	−2.617 338e+01	1.218 793e−02	− 1.894 794e−06	1
	Magnesium silicate	3.308 321e+05	− 1.391 574e+01	1.328 227e+01	7.824 586e−03	− 5.383 545e−07	
$MgTi_2O_5$(s, l)	Magnesium titanium oxide	5.804 017e+05	− 1.237 362e+01	−6.590 303e+01	1.405 198e−02	− 1.724 862e−06	1
		5.774 343e+05	9.048 780e+00	−2.071 228e+02	8.175 831e−04	− 9.154 633e−08	
$MgTiO_3$(s, l)	Geikielite	3.518 015e+05	− 9.495 908e+00	−3.177 081e+01	1.253 078e−02	− 1.924 395e−06	1
	Magnesium titanium oxide	3.494 273e+05	4.621 298e+00	−1.217 642e+02	8.711 160e−04	− 7.260 380e−08	
Mn(s, l)	Manganese	3.411 061e+04	− 2.422 703e−01	−1.619 672e+01	1.312 815e−03	3.983 368e−08	1
		3.372 262e+04	2.270 770e+00	−3.274 546e+01	3.623 250e−04	− 2.876 596e−08	
MnS(s)	Alabandite	9.064 364e+04	− 1.668 626e+00	−1.792 366e+01	8.069 930e−04	− 5.669 297e−08	5
$MnSiO_3$(s)	Pyroxmangite	3.328 499e+05	− 3.368 640e+00	−6.225 336e+01	2.116 633e−03	− 1.143 565e−07	5
N_2(s, l)	Nitrogen	1.144 108e+05	1.180 492e+01	−6.649 718e+01	− 1.623 163e−01	3.501 869e−04	7
		1.142 446e+05	6.860 148e+00	−4.814 188e+01	− 7.092 431e−02	9.991 725e−05	
N_2H_4(l)	Hydrazine	2.112 583e+05	− 5.016 141e+00	−4.552 837e+01	2.328 739e−03	1.081 899e−06	1
N_2O_4(s, l)	Nitrogen oxide	2.371 881e+05	0.000 000e+00	−9.378 900e+01	0.000 000e+00	0.000 000e+00	1
		2.153 288e+05	− 1.732 139e+02	8.442 573e+02	4.729 010e−01	− 2.076 125e−04	
NH_3(s, l)	Ammonia	1.356 675e+05	− 2.073 772e+02	8.458 273e+02	1.637 355e+00	− 2.065 313e−03	8
		1.434 961e+05	1.579 249e+00	−5.407 344e+01	− 5.959 483e−03	− 4.175 931e−06	
NH_4Cl(s)	Ammonium chloride	2.120 865e+05	− 9.628 320e+00	−2.321 631e+01	1.028 799e−02	− 1.594 689e−06	1
NH_4ClO_4(s)	Ammonium perchlorate	3.268 847e+05	− 2.461 177e+01	−7.585 352e−01	2.965 828e−02	− 4.378 953e−06	1
Na(s, l)	Sodium	1.293 288e+04	− 1.665 316e+00	−5.196 019e+00	9.504 856e−03	− 6.021 013e−06	1
		1.304 738e+04	1.729 799e+00	−2.260 327e+01	− 8.367 080e−04	1.567 141e−07	
Na_2O(s, l)	Sodium oxide	1.057 691e+05	− 2.150 694e+00	−3.539 475e+01	4.431 860e−03	− 2.177 568e−07	1
		1.018 094e+05	4.603 520e+00	−7.596 361e+01	2.082 408e−04	− 1.565 908e−08	
Na_2O_2(s)	Sodium peroxide	1.468 579e+05	− 4.310 953e+00	−4.014 897e+01	8.668 254e−03	− 1.273 752e−06	1
Na_2S(s, l)	Sodium sulfide	1.050 216e+05	8.653 401e+00	−9.818 653e+01	− 1.079 498e−02	3.035 193e−06	1
		9.800 794e+04	1.371 963e+00	−5.085 516e+01	9.718 224e−04	− 7.359 485e−08	
Na_2S_2(s, l)	Sodium sulfide	1.384 770e+05	− 1.265 367e+01	1.083 078e+01	2.874 699e−02	− 8.683 356e−06	1
		1.311 407e+05	− 1.961 069e+01	6.892 489e+01	2.154 431e−02	− 3.115 168e−06	
Na_2SO_4(s, l)	Sodium sulfate	3.426 922e+05	− 2.253 841e+01	1.010 460e+01	4.481 540e−02	− 1.098 880e−05	1
		3.434 687e+05	2.739 530e+00	−1.335 028e+02	1.716 322e−03	− 1.421 508e−07	
$Na_2Si_2O_5$(s, l)	Sodium silicate	5.773 671e+05	− 1.983 361e+01	−3.759 235e+01	2.924 649e−02	− 5.317 429e−06	1
		5.762 440e+05	− 1.864 110e+00	−1.427 231e+02	5.951 427e−03	− 5.492 852e−07	
Na_2SiO_3(s, l)	Sodium silicate	3.556 010e+05	− 1.148 912e+01	−3.428 184e+01	1.772 522e−02	− 3.178 852e−06	1
		3.455 189e+05	− 1.006 327e+01	−2.910 188e+01	8.480 798e−03	− 7.291 031e−07	
Na_3AlCl_6(s)	Sodium hexachloroaluminate	4.042 589e+05	− 8.119 085e−01	−1.511 920e+02	6.964 421e−03	− 5.080 981e−07	1
Na_3AlF_6(s, l)	Cryolite	5.324 731e+05	− 1.328 508e+01	−8.473 338e+01	2.258 069e−02	− 3.148 918e−06	1
		5.394 329e+05	1.923 886e+01	−3.009 206e+02	1.504 385e−03	− 1.149 278e−07	

Table A1 – *continued*

Species	Name	a_0	a_1	b_0	b_1	b_2	References
$Na_5Al_3F1_4$(s, l)	Chiolite	1.225 776e+06	− 1.886 442e+01	−2.513 728e+02	3.045 841e−02	− 4.387 310e−06	1
		1.254 661e+06	5.659 140e+01	−7.781 243e+02	2.631 956e−03	− 2.127 919e−07	
$NaAlCl_4$(s)	Sodium tetrachloroaluminate	2.484 835e+05	− 1.614 505e+00	−8.890 879e+01	8.297 430e−03	− 1.103 368e−06	1
$NaAlO_2$(s)	Sodium aluminum oxide	2.476 933e+05	− 4.963 382e+00	−3.828 779e+01	5.862 325e−03	− 6.164 413e−07	1
NaAlSi3O_8(s)	Albite	9.228 090e+05	− 9.591 781e−10	−2.264 186e+02	6.208 685e−13	− 4.831 038e−17	5
NaCN(s, l)	Sodium cyanide	1.678 194e+05	3.156 953e+00	−6.260 474e+01	− 6.145 218e−04	− 9.665 279e−07	1
		1.665 917e+05	1.130 587e+00	−4.909 532e+01	5.374 873e−04	− 5.037 493e−08	
$NaCO_3$(s, l)	Sodium carbonate	3.360 592e+05	− 1.103 823e+01	−3.331 982e+01	1.774 692e−02	− 3.027 202e−06	1
		3.371 626e+05	3.276 748e+00	−1.212 668e+02	2.500 792e−03	− 2.280 521e−07	
NaCl(s, l)	Halite	7.705 306e+04	− 1.494 261e−01	−2.974 098e+01	1.907 680e−03	− 2.831 117e−07	1
	Sodium chloride	7.484 593e+04	2.063 974e+00	−4.190 249e+01	5.113 600e−04	− 4.704 151e−08	
$NaClO_4$(s)	Sodium perchlorate	1.926 202e+05	− 1.053 871e+01	−4.311 559e+01	2.536 888e−02	− 5.318 760e−06	1
NaF(s, l)	Sodium fluoride	9.145 669e+04	− 1.655 268e+00	−2.236 020e+01	3.733 511e−03	− 6.749 430e−07	1
		9.037 933e+04	3.684 347e+00	−5.574 581e+01	− 2.169 080e−04	6.522 889e−09	
NaH(s)	Sodium hydride	4.530 074e+04	− 3.496 345e+00	−7.025 608e+00	5.415 961e−03	− 8.554 953e−07	1
NaO_2(s)	Sodium superoxide	1.052 766e+05	5.071 979e+00	−7.457 390e+01	− 5.291 845e−03	1.504 676e−06	1
NaOH(s, l)	Sodium hydroxide	1.196 678e+05	− 3.131 047e+00	−2.450 604e+01	1.339 562e−03	2.749 203e−06	1
		1.201 804e+05	3.258 577e+00	−6.415 605e+01	− 3.757 245e−04	5.988 784e−09	
$Ni(CO)_4$(l)	Nickel carbonyl	5.934 059e+05	1.528 607e+01	−2.138 743e+02	− 5.414 187e−02	2.804 246e−05	1
Ni(s, l)	Nickel	5.165 049e+04	− 7.770 138e−01	−1.418 381e+01	1.996 902e−03	− 3.498 124e−07	1
		5.083 042e+04	1.209 952e+00	−2.647 397e+01	2.328 150e−04	− 1.132 653e−08	
Ni_3S_2(s, l)	Heazlewoodite	2.481 926e+05	8.649 363e+00	−1.314 489e+02	− 3.562 614e−02	1.910 757e−05	1
	Nickel sulfide	2.438 967e+05	6.973 000e+00	−1.330 746e+02	1.053 581e−03	− 6.722 200e−08	
Ni_3S4(s)	Nickel sulfide	3.238 859e+05	− 5.188 410e+00	−9.446 559e+01	8.614 201e−03	1.025 834e−07	1
$NiCl_2$(s, l)	Nickel chloride	1.174 571e+05	− 1.285 269e+00	−4.301 500e+01	3.316 884e−03	− 6.381 411e−07	1
		7.809 482e+04	− 6.197 958e+01	3.779 006e+02	4.270 107e−02	− 4.583 660e−06	
NiS(s, l)	Millerite	9.505 018e+04	− 4.413 550e+00	−1.123 546e+01	8.986 445e−03	− 1.742 369e−06	1
	Nickel sulfide	9.369 626e+04	2.420 643e+00	−5.110 956e+01	6.279 077e−04	− 4.356 159e−08	
NiS_2(s, l)	Vaesite	1.339 698e+05	− 1.185 366e+00	−4.681 556e+01	1.960 389e−03	− 1.164 351e−07	1
	Nickel sulfide	1.028 536e+05	− 4.665 695e+01	2.700 304e+02	3.175 018e−02	− 3.373 018e−06	
$O_2S(OH)_2$(s, l)	Sulfuric acid	3.035 777e+05	0.000 000e+00	−1.060 685e+02	0.000 000e+00	0.000 000e+00	1
		3.006 315e+05	− 1.618 224e+01	−1.157 076e+01	2.471 556e−02	− 3.358 190e−06	
P(s, l)	Phosphorus	3.877 067e+04	8.852 251e+00	−5.893 706e+01	− 3.585 460e−02	2.356 430e−05	1
		3.813 711e+04	5.246 809e−01	−1.802 322e+01	1.462 641e−04	− 2.276 066e−08	
$(P_2O_5)_2$(s)	Phosphorus oxide	8.071 620e+05	− 3.453 923e+01	−3.775 233e+01	4.366 846e−02	− 5.766 348e−06	1
P_3N_5(s)	Phosphorus nitride	4.356 591e+05	− 1.015 124e+01	−7.275 974e+01	2.070 140e−02	− 3.157 142e−06	1
P_4S_3(s, l)	Phosphorus sulfide	2.792 320e+05	0.000 000e+00	−1.151 194e+02	0.000 000e+00	0.000 000e+00	1
		2.796 414e+05	2.959 176e+00	−1.345 227e+02	1.085 772e−03	− 1.263 153e−07	
S(s, l)	Sulfur	3.324 780e+04	8.230 502e−01	−1.915 434e+01	− 7.473 219e−03	6.541 973e−06	1
		3.414 358e+04	3.645 266e+00	−3.927 119e+01	− 2.558 100e−03	4.344 450e−07	
SCl_2(l)	Sulfur chloride	6.936 735e+04	3.233 471e+00	−5.894 255e+01	− 1.073 982e−03	3.844 648e−07	1
Si(s, l)	Silicon	5.377 075e+04	− 1.906 343e+00	−6.697 187e+00	2.855 366e−03	− 5.042 181e−07	1
		4.851 793e+04	8.361 541e−01	−2.045 829e+01	− 6.642 873e−05	1.825 015e−09	
Si_3N_4(s)	Silicon nitride, alpha	4.772 060e+05	− 9.361 923e+00	−6.235 464e+01	7.210 523e−03	− 6.175 834e−07	1
SiC(s)	Silicon carbide, beta	1.482 157e+05	− 3.559 140e+00	−1.477 158e+01	2.955 111e−03	− 2.645 741e−07	1
SiO(s)	Silicon oxide	1.451 320e+05	− 1.910 140e+00	−2.029 867e+01	6.185 105e−04	− 4.216 349e−08	9
SiO_2(s, l)	Silicon dioxide	2.225 032e+05	− 5.492 533e+00	−2.075 544e+01	6.331 284e−03	− 9.105 538e−07	10
		2.185 727e+05	− 6.967 639e+00	−5.420 608e+00	3.986 627e−03	− 2.747 098e−07	
SiS_2(s, l)	Silicon sulfide	1.465 184e+05	− 2.740 423e−01	−5.035 944e+01	2.283 212e−03	− 2.893 822e−07	1
		1.231 541e+05	− 3.994 238e+01	2.255 866e+02	2.545 788e−02	− 2.489 610e−06	
Ti(s, l)	Titanium	5.677 155e+04	− 1.227 259e+00	−1.096 439e+01	2.166 856e−03	− 2.322 204e−07	1
		5.977 556e+04	4.249 729e+00	−4.990 116e+01	− 3.932 996e−04	2.304 430e−09	
Ti_2O_3(s, l)	Titanium oxide	3.847 074e+05	− 1.095 307e+01	−2.764 763e+01	1.664 392e−02	− 2.602 469e−06	1
		3.750 538e+05	2.502 303e+00	−1.047 853e+02	1.357 783e−03	− 1.225 017e−07	
Ti_3O_5(s, l)	Titanium oxide	6.136 540e+05	− 1.483 965e+01	−5.925 200e+01	2.465 791e−02	− 4.287 191e−06	1
		6.049 721e+05	8.774 242e+00	−2.040 415e+02	1.095 428e−03	− 1.227 866e−07	
Ti_4O_7(s, l)	Titanium oxide	8.457 487e+05	− 8.810 282e+00	−1.475 694e+02	1.359 895e−02	− 1.740 277e−06	1
		8.376 337e+05	1.408 512e+01	−2.981 153e+02	8.591 056e−04	− 1.320 712e−07	
TiC(s, l)	Titanium carbide	1.645 199e+05	− 3.261 366e+00	−1.755 256e+01	3.346 973e−03	− 3.490 044e−07	1
		1.633 484e+05	6.162 907e+00	−8.301 350e+01	− 1.081 446e−03	3.146 153e−08	
$TiCl_2$(s)	Titanium chloride	1.478 096e+05	− 2.010 910e+00	−3.934 015e+01	3.484 307e−03	− 3.868 436e−07	1
$TiCl_3$(s)	Titanium chloride	1.878 227e+05	7.714 631e−01	−6.992 851e+01	3.094 332e−04	1.335 437e−07	1
$TiCl_4$(s, l)	Titanium chloride	2.125 171e+05	0.000 000e+00	−7.629 495e+01	0.000 000e+00	0.000 000e+00	1
		2.131 810e+05	3.813 615e+00	−1.000 270e+02	− 3.217 674e−05	2.045 416e−07	
TiF_3(s)	Titanium fluoride	2.580 094e+05	− 1.644 778e+00	−5.896 958e+01	2.724 400e−03	− 1.479 247e−07	1
TiF_4(s)	Titanium fluoride	2.923 188e+05	− 7.799 828e+00	−3.748 423e+01	1.435 265e−02	− 2.549 007e−06	1

Table A1 – *continued*

Species	Name	a_0	a_1	b_0	b_1	b_2	References
TiH_2(s)	Titanium hydride	1.249 501e+05	− 8.105 000e+00	4.4282 71e+00	7.428 109e−03	− 9.777 304e−07	1
TiN(s, l)	Titanium nitride	1.537 865e+05	− 2.703 635e+00	−1.981 151e+01	3.014 155e−03	− 3.107 625e−07	1
		1.307 269e+05	− 1.079 465e+01	5.022 860e+01	3.293 668e−03	− 1.553 395e−07	
TiO(s, l)	Titanium oxide	1.514 670e+05	− 3.675 177e+00	−1.482 323e+01	4.743 702e−03	− 5.181 798e−07	1
		1.491 392e+05	3.610 219e+00	−6.116 719e+01	− 2.254 299e−04	− 7.164 901e−09	
TiO_2(s, l)	Rutile	2.293 679e+05	− 5.579 366e+00	−2.061 548e+01	6.888 392e−03	− 1.023 248e−06	1
	Titanium oxide	2.279 416e+05	2.995 753e+00	−7.643 098e+01	4.869 790e−04	− 4.665 479e−08	
V(s, l)	Vanadium	6.178 073e+04	− 1.058 384e+00	−1.210 524e+01	1.460 874e−03	− 1.709 780e−07	1
		6.258 078e+04	1.907 257e+00	−3.350 554e+01	3.464 223e−04	− 2.916 535e−08	
V_2O_3(s, l)	Karelianite	3.594 059e+05	− 4.525 272e+00	−6.248 195e+01	5.547 256e−03	− 5.116 554e−07	1
	Vanadium oxide	3.430 939e+05	− 2.182 166e+00	−6.895 187e+01	2.726 860e−03	− 1.688 924e−07	
V_2O_4(s, l)	Vanadium oxide	4.138 200e+05	− 7.706 466e+00	−6.324 071e+01	1.428 494e−02	− 2.749 633e−06	1
		4.006 761e+05	− 7.197 933e+00	−5.418 588e+01	7.151 172e−03	− 5.011 278e−07	
V_2O_5(s, l)	Shcherbinaite	4.580 524e+05	− 1.240 157e+01	−5.194 057e+01	1.863 388e−02	− 3.815 827e−06	1
	Vanadium oxide	4.536 238e+05	4.659 504e−01	−1.230 467e+02	2.126 091e−03	− 1.807 118e−07	
VN(s)	Vanadium nitride	1.443 584e+05	− 2.457 896e+00	−2.053 464e+01	2.367 187e−03	− 1.939 530e−07	1
VO(s, l)	Vanadium oxide	1.432 838e+05	− 3.129 339e+00	−1.797 255e+01	4.472 298e−03	− 6.021 079e−07	1
		1.345 012e+05	− 1.960 904e+00	−1.874 037e+01	1.567 102e−03	− 1.023 190e−07	
Zn(s, l)	Zinc	1.575 906e+04	− 1.232 552e−01	−1.428 515e+01	1.436 668e−03	− 3.507 159e−07	1
		1.527 125e+04	1.050 780e+00	−2.053 114e+01	1.544 112e−04	− 1.683 046e−08	
$ZnSO_4$(s)	Zinc sulfate	2.841 321e+05	− 1.432 225e+01	−1.911 778e+01	2.033 870e−02	− 3.227 622e−06	1

References: (1) Chase (1998); (2) Moses, Allen & Yung (1992), Prydz & Goodwin (1972), NIST Chemistry Webbook; (3) Goodwin (1985); (4) Yaws (1999), NIST Chemistry Webbook; (5) Sharp & Huebner (1990); (6) Murphy & Koop (2005), Wagner & Kretzschmar (2008); (7) Dykyj et al. (2001); (8) Lide (2009), Haar & Gallagher (1978); (9) Gail et al. (2013); and (10) Barin (1995).

As stated by Stock et al. (2018), we parametrize $\ln \bar{K}_c$ as a function of the temperature T in form of the polynomial

$$\ln \bar{K}_c(T) = \frac{a_0}{T} + a_1 \ln T + b_0 + b_1 T + b_2 T^2 \,, \tag{A6}$$

where a_i and b_i are the corresponding fit coefficients that are tabulated in the FASTCHEM input file for each species.

Following the approach of the gas phase data in the previous versions of FASTCHEM, we base our choice of species mainly on the JANAF tables (Chase 1998). In particular, we use all condensates for the elements contained in FASTCHEM included in the JANAF tables. Species that have both liquid- and solid-form data are fitted independently. Thus, some condensate species have two different sets of polynomial coefficients attached to them. FASTCHEM COND in principle allows a condensate with a certain stoichiometric formula to have even more sets of fit coefficients. It is, thus, possible to fit also different crystal phases independently if so desired by the user. A list of all species and the fit coefficients can be found in Table A1.

In addition to the JANAF tables, we also add selected condensates from other data sources. This includes condensate species from Sharp & Huebner (1990) not available in the JANAF tables, some volatile, low-temperature condensates such as water, ammonia, methane, or carbon dioxide, and silicon monoxide [SiO(s)] from Gail et al. (2013).

For species where the thermochemical data are given in terms of the saturation vapour pressure $p_{\mathrm{vap},c}(T)$ rather than the Gibbs free energy, we use the relation

$$\ln\left(\frac{p_{\mathrm{vap},c}(T)}{p^{\ominus}}\right) = \frac{G_c^{\ominus}(T) - G_i^{\ominus}(T)}{RT} \tag{A7}$$

to calculate $G_c^{\ominus}(T)$, where $G_i^{\ominus}(T)$ is the Gibbs free energy of the corresponding molecule. For the latter, we again use the gas phase data from the JANAF tables.

We note that we exchanged the data for SiO_2(s, l) from the JANAF tables with that from Barin (1995). The JANAF data suggest that SiO_2(l) would switch into solid SiO_2, more specifically quartz, at a temperature of 1696 K. However, the standard phase diagram of SiO_2 as well as the data from Barin (1995) or the NASA Glenn coefficients (McBride, Zehe & Gordon 2002) all agree that at standard pressure, SiO_2(l) first transitions into the solid cristobalite at a temperature of 1996 K before its stable form finally changes to quartz at lower temperatures. Due to the discrepancies between the JANAF tables and the other literature, we choose to use the data from Barin (1995) instead.

Thermochemical data for condensates are often only available over a very restricted temperature range. Therefore, by default, FASTCHEM COND avoids extrapolating the fit equation (A6) outside of the temperature range of the underlying data. A special configuration parameter is available in FASTCHEM COND, though, that allows the user to override this limitation. However, this parameter should only be used with great care as the extrapolation might result in an unphysical, non-monotonic behaviour of the $\ln K_c$ fit for some condensate species.

APPENDIX B: ELEMENT–CONDENSATE MAPPING

In order to determine the correlation between the condensed species and their associated elements even at the highest number of possible stable condensates according to the phase rule, one can apply a simple scheme that is briefly discussed in the following. The scheme is applied to the outermost region of the protoplanetary disc from Section 4.2 and its results are summarized in Table 1.

Fig. B1 depicts the end result of how a unique mapping between the chemical elements and their corresponding condensates according to the phase rule can be found. The figure defines a matrix, which entries are '1', if the condensate contains the respective element. The number in the outermost left column on the left-hand side of the figure indicates how many condensates an element can be associated with. The elements are then sorted by this number, e.g. carbon receives a '1', because the only condensate containing carbon is CH_4, nitrogen receives a '2', because NH_4Cl and NH_3 include nitrogen, and so on. The mapping of the elements C, Ca, ..., Zn is

already determined, since they have only one condensate to associate with. These condensates are therefore not available to other elements. In the next step, the numbers on the left-hand side in Fig. B1 are updated accordingly (second column). The procedure is repeated until no condensate is left.

In our example, the final condensate is H_2O, which can be assigned to either hydrogen or oxygen, since the total number of elements exceeds the total number of condensates by one. If a bijective mapping is desired, a secondary criterion must be utilized, such as, for example, the stoichiometrically normalized element abundance. In this case, we would assign oxygen, the less abundant element, to H_2O. Note that the domain of the mapping must then be reduced by hydrogen that is left over. The described algorithm works because the condensates are linearly independent (see Sections 2.3 and 3).

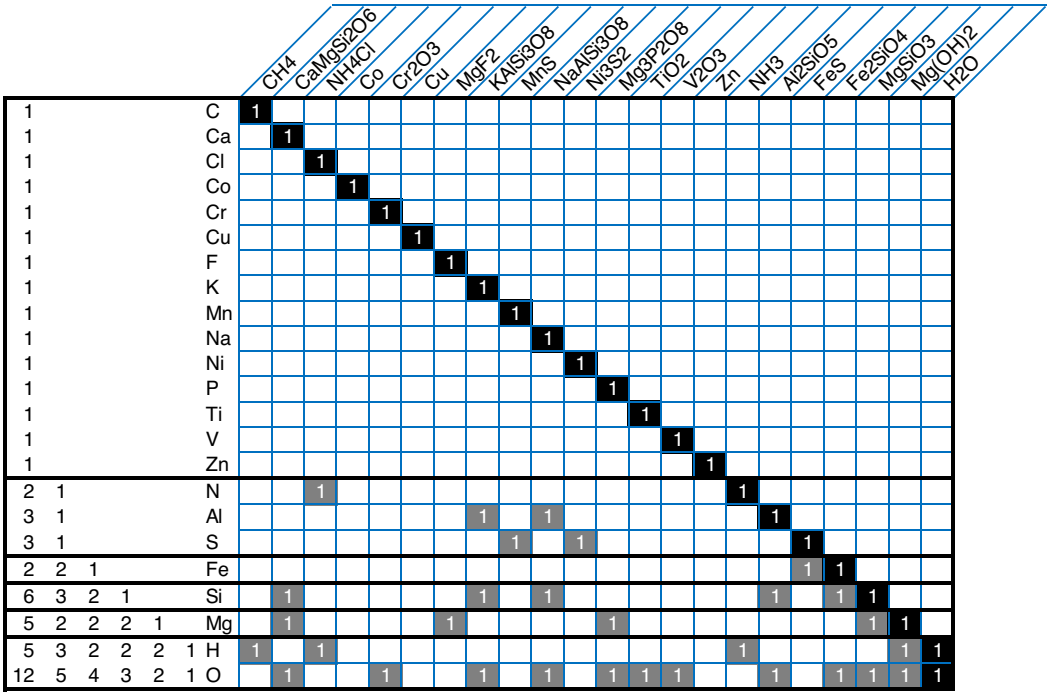

Figure B1. Mapping between the chemical elements and their corresponding condensates according to the phase rule (see text for details).

This paper has been typeset from a TEX/LATEX file prepared by the author.